

Award Number: **W81XWH-10-1-0733**

TITLE: **Systems-Level Analysis of EGFR Inhibition-DNA Damage Combination Treatment in Breast Cancer**

PRINCIPAL INVESTIGATOR: **Michael J. Lee, Ph.D.**

CONTRACTING ORGANIZATION: **Massachusetts Institute of Technology
Cambridge, MA 02139**

REPORT DATE: **September 2012**

TYPE OF REPORT: **Annual Summary**

PREPARED FOR: **U.S. Army Medical Research and Materiel Command
Fort Detrick, Maryland 21702-5012**

DISTRIBUTION STATEMENT: **Approved for Public Release;
Distribution Unlimited**

The views, opinions and/or findings contained in this report are those of the author(s) and should not be construed as an official Department of the Army position, policy or decision unless so designated by other documentation.

REPORT DOCUMENTATION PAGE				Form Approved OMB No. 0704-0188	
Public reporting burden for this collection of information is estimated to average 1 hour per response, including the time for reviewing instructions, searching existing data sources, gathering and maintaining the data needed, and completing and reviewing this collection of information. Send comments regarding this burden estimate or any other aspect of this collection of information, including suggestions for reducing this burden to Department of Defense, Washington Headquarters Services, Directorate for Information Operations and Reports (0704-0188), 1215 Jefferson Davis Highway, Suite 1204, Arlington, VA 22202-4302. Respondents should be aware that notwithstanding any other provision of law, no person shall be subject to any penalty for failing to comply with a collection of information if it does not display a currently valid OMB control number. PLEASE DO NOT RETURN YOUR FORM TO THE ABOVE ADDRESS.					
1. REPORT DATE FÄÜ] c\ à\ 2012		2. REPORT TYPE Annual Summary		3. DATES COVERED FÄÜ] 2011ÄÄFÄE * 2012	
4. TITLE AND SUBTITLE Systems-Level Analysis of EGFR Inhibition-DNA Damage Combination Treatment in Breast Cancer				5a. CONTRACT NUMBER	
				5b. GRANT NUMBER Y I FYY PÉÉÉ HÄ	
				5c. PROGRAM ELEMENT NUMBER	
6. AUTHOR(S) Michael J. Lee, Ph.D. E-Mail: mikejlee@mit.edu				5d. PROJECT NUMBER	
				5e. TASK NUMBER	
				5f. WORK UNIT NUMBER	
7. PERFORMING ORGANIZATION NAME(S) AND ADDRESS(ES) Massachusetts Institute of Technology Cambridge, MA 02139-4301				8. PERFORMING ORGANIZATION REPORT NUMBER	
9. SPONSORING / MONITORING AGENCY NAME(S) AND ADDRESS(ES) U.S. Army Medical Research and Materiel Command Fort Detrick, Maryland 21702-5012				10. SPONSOR/MONITOR'S ACRONYM(S)	
				11. SPONSOR/MONITOR'S REPORT NUMBER(S)	
12. DISTRIBUTION / AVAILABILITY STATEMENT Approved for Public Release; Distribution Unlimited					
13. SUPPLEMENTARY NOTES					
14. ABSTRACT Triple-negative breast cancer (TNBC) is a heterogeneous mix of cancers defined only by the absence of the three best-characterized prognostic markers: estrogen receptor (ER), progesterone receptor (PR), and the human epidermal growth factor receptor 2 (HER2). This lack of understanding underlies our inability to identify effective therapeutic options for these patients. During the previous research period for this award (year 1), we identified that a subset of TNBCs have high baseline levels of activated EGFR, and were sensitive to certain temporal combinations of EGFR inhibition and DNA damaging chemotherapy. The focus of this research period (year 2) was to determine the mechanism of this enhanced sensitivity to chemotherapy. Using an integrative analysis of multiple signaling networks, we identified that chronic exposure to EGFR inhibition in a subset of TNBCs resulted in a profound genetic rewiring, resulting in more than 2000 differentially expressed genes (DEGs). Further analyses revealed that caspase-8 played a crucial role in the combination therapy we identified, a surprising and unexpected finding, since this protein was not previously thought to contribute to DNA damage-induced cell death. Collectively, these findings identify a novel method for enhancing chemotherapeutic efficacy, through rewiring apoptotic signaling networks.					
15. SUBJECT TERMS DNA damage response; systems biology; triple-negative breast cancer					
16. SECURITY CLASSIFICATION OF: U			17. LIMITATION OF ABSTRACT UU	18. NUMBER OF PAGES 62	19a. NAME OF RESPONSIBLE PERSON USAMRMC
a. REPORT U	b. ABSTRACT U	c. THIS PAGE U			19b. TELEPHONE NUMBER (include area code)

Table of Contents

	Page
Introduction.....	4
Body.....	5
Key Research Accomplishments.....	20
Reportable Outcomes.....	20
Conclusions.....	21
References.....	23
Appendices.....	25
Supporting Data.....	45

INTRODUCTION

Decades of research have revealed cancer to be a remarkably complex disease, with profound heterogeneity existing between patients, between the tumors of a single patient, and even between the malignant cells within a single tumor (Hanahan and Weinberg, 2011). Responding to this complexity, many have rightly cited the need for more personalized therapies; however, it is still not clear what cellular, molecular, or tumor micro-environmental factors need to be considered for optimal patient stratification (Dancey et al., 2012). This is particularly a problem for triple-negative breast cancers (TNBCs), a heterogeneous subtype that represents about 20% of all cases (Bosch et al., 2010). The term “triple-negative” clearly reflects our lack of understanding about this disease, as these tumors are defined only by the absence of estrogen receptor, progesterone receptor, and amplified HER2. Patients with this disease generally have shorter relapse-free survival rates and a worse overall prognosis than other breast cancer patients. Currently, there are no targeted therapies for TNBC, a direct consequence of our lack of molecular information about these cancers. My previous work helped to identify that a subset of TNBC cells have perturbed EGFR signaling, and furthermore, we developed a treatment strategy for potentiating the effects of chemotherapy in these cells (Figure 1). The goal of this current work is to gain a molecular understanding of the enhanced chemosensitivity that we observed in TNBC cells, determine to what extent this phenomenon is unique to TNBC, and use this information to advance the development of targeted therapies for TNBCs and other malignancies.

BODY

AIM 1: Identify optimal co-treatments of ErbB receptor inhibitors with various DNA damaging agents in a panel of established breast cancer cells

The work proposed under Aim 1 of this proposal was completed during the previous research phase of this award and summarized in the Annual Summary for year 1 of this research program. Briefly, we screened various combinations of targeted inhibitors with DNA damaging chemotherapeutic agents in a panel of triple-negative breast cancer (TNBC) cells. This screen identified that certain temporally staggered combinations of erlotinib and doxorubicin were synergistic in eliciting cell death. The most efficacious of these were those combinations in which erlotinib was given between 4 and 24 hours before doxorubicin. See the Annual Summary for 2011 for more details.

AIM 2: Interrogate the integrated EGFR-DNA damage network in breast cancer cells following erlotinib (Tarceva) – doxorubicin (Adriamycin) combination treatment

Following DNA damage, cells initiate a complex cascade of signaling responses to coordinate the machinery necessary for DNA repair (Harper and Elledge, 2007). This typically involves arresting the cell cycle and, if the damage is too severe, activating apoptotic programs to remove the cell. In cancer cells, the DNA Damage Response (DDR) has invariantly been perturbed to some extent to allow for tumor progression. Since many of our efficacious anti-cancer therapies function by causing DNA damage-induced cell death, the atypical DDR signaling that can exist in cancerous cells often leads to unpredictable responses and resistance to therapy. Furthermore, recent evidence suggests that DNA damage signaling utilizes a network much larger than

previously considered (Tentner et al., 2012). Thus, gaining a comprehensive understanding how DNA damage signaling occurs in various subtypes of breast cancer should help inform future therapeutic alternatives. The goal of this aim was to broadly measure signaling responses following erlotinib/doxorubicin combination treatments. These measurements were made in cells where the combinations were efficacious as well as those in which the combinations were inefficacious, allowing us to infer which pathways or proteins were critically involved in the cellular responses we monitored.

Task 4. Probe lysates to gain insight into signaling states using quantitative techniques

The long-term goal for this project is to create a data-driven computational model of the DNA damage response in various subtypes of breast cancer, as detailed in Aim 3 of this proposal. For these types of models, predictions can only be made about that which was measured, so model performance is critically dependent on selecting and measuring the correct proteins for analysis. Our strategy for selecting targets of interest had 3 distinct phases. The first phase was to curate a list of proteins involved in DNA damage response, using the broadest definition. The second phase was to identify and validate antibodies for use in our quantitative high-throughput experiments. Both of these phases were discussed in the previous Annual Report (pages 10-11). The third phase was to identify list of proteins that may be involved with the chemosensitivity that we had observed, using methods that do not rely on prior knowledge. This aspect was critical in order to identify novel components of DNA damage signaling that may be relevant to breast cancer therapy.

Identification of Protein Targets of Interest. To identify proteins that could be involved in our time-staggered erlotinib/doxorubicin treatment, we utilized the fact that enhancing chemosensitivity with erlotinib required many hours of exposure. Our rationale was that long-term exposure to erlotinib may be necessary to allow time for adaptive/compensatory changes in gene expression. Thus, we performed a series of gene microarray experiments to identify the global changes in gene expression following erlotinib treatment. In triple-negative BT-20 cells, EGFR inhibition for 30 minutes resulted in only a few differentially expressed genes (DEGs) (Figure 2A). Following 6 hours of erlotinib treatment, however, we observed over 1200 DEGs, and following 24 hours of treatment, when doxorubicin sensitivity was maximally enhanced, we observed over 2000 DEGs (Figure 2B-C). By comparison, in the HER2+ MDA-MB-453 cells, which were desensitized to doxorubicin by erlotinib exposure, we observed only 235 DEGs following 24 hour exposure to erlotinib, and in hormone-sensitive MCF7 cells only one gene was significantly altered (Figure 2D-E). Thus, the triple-negative BT-20 cells exhibited progressive and large-scale changes in gene expression following EGFR inhibition that were not observed in cell lines insensitive to the time-staggered ERL→DOX combination. This was consistent with our hypothesis that altered gene expression could account for the time-dependent efficacy seen in the BT-20 cells.

To examine which cellular processes were altered by long-term erlotinib treatment (which would inform which particular protein targets that need to be monitored), DEGs in BT-20 cells were categorized by cellular process according to the GeneGO pathway annotation software (Ekins et al., 2007). The GeneGO software package includes hundreds of annotated signaling pathways, which are grouped into 34

“cellular processes” which collectively cover most, if not all, cellular functions. Significant changes were observed in 16 of 34 GeneGO cellular networks, including those that mediate the DDR, apoptosis, and inflammation (Figure 3). In contrast to what was seen in TNBC cells like BT-20, the DEGs in MDA-MB-453 were not only fewer in number, but also lay in networks that did not overlap with those altered in BT-20 (Figure 3). These data highlight the uniqueness of the response seen in the triple-negative BT-20 cells exposed to erlotinib and also provided insight into which networks had changed significantly.

As a complimentary method, we also analyzed gene expression data using Gene Set Enrichment Analysis (GSEA), a tool for identification of enrichment or depletion of defined gene expression signatures within a rank ordered gene list (Tamayo et al., 2011). The most statistically significant changes in BT-20 cells upon sustained erlotinib exposure were loss of the Ras and MYC oncogenic signatures (Figure 4). These signatures were not significantly altered in MDA-MB-453 or MCF7 cells treated with erlotinib for 24 hours, or in BT-20 cells exposed to erlotinib for 30 minutes (Figure 4). Within the GSEA molecular signatures database, there exist 11 oncogenic signatures (Subramanian et al., 2005). GSEA of EGFR-inhibited BT-20 cells showed a similar depletion pattern for all 11 oncogenic signatures (Figure 4). These changes were not consistently observed in either MDA-MB-453 cells or MCF7 cells following exposure to erlotinib.

In addition to the gene signatures, GSEA also can perform an analysis called cancer gene network analysis (CGN). CGN defines a cancer gene network as those genes whose expression is covaries with the expression of any of the 380 most well

characterized cancer genes (i.e. tumor suppressors and oncogenes). Thus changes in a cancer gene network may suggest an involvement of a known cancer gene. Since our GSEA revealed that oncogenic gene expression signatures were being altered, we used CGN to identify which cancer genes were likely to be targeted. Using CGN analysis, we identified two networks as being of potential interest: ATM and Caspase-8 (Figure 5). In other words, CGN analysis revealed that the pattern of DEGs in BT-20 cells was similar to a list of genes whose expression changes when ATM is perturbed, or when caspase-8 is perturbed. Both of these were surprising. ATM is a well-known DNA damage response protein, however, since these cells had not been exposed to any DNA damaging agents at the time of analysis, we did not expect perturbation of the ATM network. Caspase-8 was even more surprising. While caspase-8 is a known pro-apoptotic initiator protein, it was not thought to be involved in DNA damage induced apoptosis. The traditional role for caspase-8 is in regulation of death receptor induced apoptosis (i.e. the cell “extrinsic” apoptotic pathway). DNA damage, on the other hand, is thought to utilize caspase-9 (i.e. the cell “intrinsic” apoptotic pathway). Furthermore, ATM would likely have been on our list of targets of interest because of its established role in DNA damage signaling, however, caspase-8 was not previously on our list of targets. In summary, we compiled a list of protein targets of interest by identifying altered signaling pathways (using GeneGO), known genetic signatures (GSEA), and altered cancer gene networks (CGN). The total list of protein targets of interest, as well as the source for identification, is listed in Table 1.

For the signaling measurements and analyses described below, we hypothesized that a signaling response was worthy of more direct interrogation if one of the following

criteria were fulfilled: 1) the response pattern (i.e. increase or decrease in the activity or expression) was unique to the erlotinib→doxorubicin “pre-treatment” condition in BT-20 cells; 2) the response pattern was modulated by the order and timing of drug presentation; or 3) the response pattern differed across the cell line panel. In our view, the first criterion would be the most indicative of signals that were likely to be specifically involved in driving enhanced chemosensitivity following long-term exposure to erlotinib. In addition to this first line analysis, we also are planning to use these data to build multivariate regression models. These models will allow us to make predictions about more complex combinatorial effects that may exist in the dataset. This work is described in Aim 3 of the proposal, and will occur during Year 3 of the award period as detailed in the Statement of Work. The data for each of the signaling measurements we made is summarized below, as delineated in Aim 2 of the proposal in Task 4 of the Statement of Work.

EGFR/ErbB Pathways. The EGFR pathway is typically thought to consist of two main branches: the “Ras – Raf – Mek – Erk” arm and the “PI3K – AKT” arm (Figure 6). Since erlotinib targets EGFR directly, both of these signaling branches were of interest for our analyses. These data are shown in Figure 7. Not surprisingly, EGFR and/or HER protein levels were unchanged by any of our treatments in any cell line. Phosphor-EGFR (Y1173) was responsive to erlotinib but not doxorubicin. Erlotinib induced a rapid and sustained loss of EGFR phosphorylation. Other signals that we measured were less clearly associated with erlotinib or doxorubicin sensitivity. For example, p-MEK, p-ERK, and p-AKT were each inhibited by erlotinib and induced by doxorubicin. When the

two drugs were combined, in each case the erlotinib-mediated inhibition was dominant over the doxorubicin-mediated activation, and this phenomenon was independent of the timing of drug addition. In general, the activity levels were much lower in MCF7 cells when compared to MDA-MB-453 or BT-20. The one exception was DUSP6, a dual specificity phosphatase that is known to inactivate ERK and other substrates. DUSP6 expression was generally low, but was very high in MCF7 cells. An interesting example from this portion was JNK, a known stress-activated kinase. Our data show that JNK responds to these drugs in a very cell line specific manner. In BT-20 cells, JNK was induced strongly by doxorubicin, but unchanged in the erlotinib treatment condition. Interestingly, all combinations in BT-20 that contained erlotinib and doxorubicin did not induce JNK signaling, regardless of drug timing. Alternatively, in the MCF7 cells JNK was always induced by doxorubicin, regardless of the presence or absence of erlotinib, and in the M453 cells, JNK was not robustly induced by any treatment. Other signals that we measured (B-Raf, p90RSK, p-SEK, p-ABL) were unchanged by any treatment in any cell line. Thus as a whole, ErbB signaling was modulated by erlotinib and doxorubicin treatments. No signals were observed to change specifically in the synergistic pre-treatment drug condition. Cell line specific signaling patterns were observed for ERK, JNK, and DUSP6. These responses will be the focus of further analysis in the next research period.

DNA Damage Pathways. Many proteins are known to respond to DNA damage signals, including proteins involved in sensing DNA breaks, DNA repair proteins, general stress response proteins, cell cycle proteins, and a number of kinases

responsible for transducing and amplifying the signal (Harper and Elledge, 2007). Here, we focused on well-established members of the DNA damage response, critical mediators of DNA damage-mediated cell cycle arrest, and proteins involved with DNA repair. One major hurdle here was the identification of high-fidelity antibodies (the process for antibody validation was described in the Annual Summary for Year 1 of this award). Many important targets simply could not be measured quantitatively using the reagents available to us. As a complimentary approach, new reagents are being developed, as described in Task 5 below. These data are shown in Figure 8. In general, stimulus-dependent changes were observed for doxorubicin treated but not erlotinib treated conditions. Also, combinations of doxorubicin and erlotinib (regardless of drug timing) were generally not different that doxorubicin alone. This included H2AX, p53 (total and phosphorylated at Ser15 or Ser20), p-Chk1, p-Chk2, p-Hsp27, p-p38. Furthermore, we did not observe stimulus dependent changes in repair proteins p-DNA-PKcs, p-BRCA1, or p-53BP1. We speculate that the lack of DNA repair responses in our dataset result from the relatively high dose of damage (10uM doxorubicin) and relatively short observation window (most measurements were made in the first 8 hours after treatment). At these doses and times, damage may have been too severe for cell cycle arrest/repair, and cells may be biased towards apoptotic responses. Taken together, the signaling trajectories we observed imply that the differences in drug efficacy that we observed do not arise from differences in the canonical portion of the DNA damage response or from differences in DNA repair.

Because we found these data surprising, we further confirmed that DNA damage accumulation was similar in all doxorubicin/erlotinib conditions. Some membrane

pumps can be modulated by EGFR inhibitors and are responsible for multi-drug resistance in at least some breast cancer. We therefore measured the intracellular accumulation of doxorubicin by flow cytometry and found that prior treatment with erlotinib did not alter the intracellular doxorubicin concentration (Figure 9A-D). Next as pharmacodynamic markers of doxorubicin action we assayed two indicators of DNA double stranded breaks: phosphorylation of histone H2AX at S139 and formation of 53BP1-containing nuclear foci. Both assays showed similar responses across all treatment conditions (Figure 9E-H). Taken together, these data indicate similar levels of DNA damage and early DNA damage-related signaling in DOX and ERL→DOX treated cells, independent of the efficacy of the combination in cell killing. These data imply that differential levels of cell death result do not result from more DNA damage, or even more DNA damage signaling, but likely from rewiring signaling pathways.

Cell Cycle Pathways. In our signaling dataset, while stimulus dependent changes were not generally observed, likely for the reasons described above. The one exception was phosphor-Histone H3 (pHH3), a marker of mitosis. In all cases, doxorubicin treatment resulted in loss of pHH3, indicating a DNA damage induced G2 arrest that is commonly seen in doxorubicin treated cells (Tentner et al., 2012). Nearly all targets measured displayed levels that were unique to that cell line (Figure 11). For example, p-Wee1 and p-Cyclin D1 were high in BT-20 and MDA-MB-453 cells, but low in MCF7; and p27 was low in BT-20 and MCF7, but high in MDA-MB-453. No differences were observed for p-Cdc25 or cyclin E. As described above, the various drug combinations we tested were given at relatively high concentrations, inducing

strong DNA damage signaling and cell death. Thus, cell cycle modulation may not play a critical role in this response.

The one outlier to this generality was seen in HER2 over-expressing MDA-MB-453 cells subject to the erlotinib→doxorubicin treatment. These cells had less DNA damage signaling when compared to the other treatment conditions that had both erlotinib and doxorubicin (see Figure 8). This would be consistent with long-term erlotinib exposure resulting in cell cycle arrest in a portion of the cell cycle that was less sensitive to DNA damage (G1 for example rather than S). To test this, we monitored cell cycle progression using flow cytometry in each cell line in our panel. Indeed, significantly fewer cells were in S-phase in MDA-MB-453 cells treated with ERL→DOX, compared to DOX/ERL or DOX→ERL conditions (Figure 10B). In the other cell lines, although doxorubicin and erlotinib altered cell cycle dynamics depending on the cell type, cells that received both drugs had similar cell cycle profiles regardless of the dosing regimen (Figure 10A and C); in particular, there is no evidence that cells exposed to the ERL→DOX protocol accumulate in S/G2, the cell cycle stage where doxorubicin may be most effective. Thus, cell cycle modulation cannot explain the unique efficacy of sequential drug exposure, but may explain the antagonism of ERL→DOX in the MDA-MB-453 cells.

Apoptotic Pathways. Cellular apoptosis is typically divided into two pathways: the cell-intrinsic and cell extrinsic responses. The cell-intrinsic response is primarily regulated by BID truncation and cytochrome c release from mitochondria, resulting in cleavage and activation of caspase-9 (Green and Evan, 2002). This form of cell death

is thought to be the primary form responsible for DNA damage induced cell death (Zinkel et al., 2005). Alternatively, the cell-extrinsic pathway is regulated by death receptor binding to ligands like TNF or TRAIL and activation of caspase-8 (Galluzzi et al., 2011). Challenging this traditional view, evidence is beginning to emerge that these two pathways share significant ability to cross-talk (Albeck et al., 2008). Nonetheless, traditional chemotherapeutics like doxorubicin have not been reported to activate the cell-extrinsic pathway. Our genetic data (described above) identified that the caspase-8 genetic network was robustly changed following long-term exposure to erlotinib. This change only occurred in BT-20 cells.

A summary of our apoptotic signaling dataset is shown in Figure 12. In general there were no apoptotic signals resulting from erlotinib treatment alone, and some known apoptotic regulators had similar levels in all treatment conditions in all cell lines (cIAP1, cIAP2, XIAP). Notably however, BID, which was generally low in all cells, was induced after long-term exposure to erlotinib in BT-20 cells. This was not unique to the pre-treatment condition but warrants further experimentation. We observed cell line specific protein levels for many signals including BID, SMAC, RIP, and PUMA. Because each of these proteins are known pro- and anti-apoptotic regulators, their relative stoichiometric ratios are likely to help dictate the apoptotic threshold, thus each of these proteins will be the focus of future analyses during the modeling phase of our project.

As expected caspase-3, and -9 were induced by doxorubicin, but the levels of caspase-9 in particular did not correlate with the levels of death observed. Surprisingly, caspase-6 was robustly activated in treatment conditions that resulted in synergistic

levels of cell death, including ERL→DOX treatment in BT-20 cells, and DOX/ERL and DOX→ERL treatment in MDA-MB-453. Furthermore, caspase-8 was uniquely activated in the ERL→DOX treatment in TNBC BT-20 cells, the combination that is of the most interest in our analysis.

In our initial planning, we deemed that the most interesting signals would be those that were uniquely activated in the ERL→DOX condition in the TNBC BT-20 cells. In our entire dataset, caspase-8 was one of the only signals to meet that criterion. Thus, we were interested in directly testing the hypothesis that caspase-8 activation was responsible for the enhanced apoptosis that we observed. To test this prediction experimentally, 2 separate caspase-8 siRNAs were used in both BT-20 cells and MDA-MB-453 cells (Figure 13). Knockdown of caspase-8 mitigated the enhanced cell death following erlotinib treatment in BT-20 cells, while having minimal effect on apoptosis following other treatment combinations. Furthermore, caspase-8 knockdown had little effect on apoptosis in MDA-MB-453 under any condition. Thus caspase-8 appears to play a unique role in driving the enhanced apoptotic response seen in BT-20 cells treated with the ERL→DOX combination.

Autophagy/Metabolic Pathways. One of the main focuses of this proposal was to investigate the role of autophagy in the chemosensitivity of breast cancer cells. Recent evidence suggests that autophagy may be involved in modulating cell death responses, however, the exact role for autophagy in this context is still unclear (Levine, 2005; Jin and White, 2007). We measured signals known to regulate autophagy, as well as the formation of LC3-positive vesicles which are indicative of positive autophagic flux

(Figure 14) (Mizushima et al., 2010). LC3 analysis showed clearly that doxorubicin treatment causes an increase in autophagic flux in all of our cell lines (data included in Year 1 Annual Summary). No treatment dependent changes were observed for beclin-1, ATG5 or ATG12, all proteins known to be required for autophagy. The best-known regulator of autophagy is mTOR and its downstream signaling. Unfortunately, we were unable to reliably measure mTOR itself. mTOR is a large protein (which typically do not transfer well for western blot analyses), and none of the available phosphorylation-specific antibodies for mTOR were functional in our system. We were, however, able to measure activation states of proteins known to be downstream of mTOR, like 4E-BP1, s6-kinase, and s6. For all of these proteins, erlotinib exposure in BT-20 and MDA-MB-453 cells resulted in decreased activity, while doxorubicin had no effect. MCF7 cells had very low levels of pathway activation downstream of mTOR and each of these proteins was unresponsive to both erlotinib and doxorubicin.

Other pathways that have been associated with modulation of autophagy are the NF-kB pathway, the JAK/STAT signaling, and the death associated protein kinases (DAPKs). IKBs inhibit NF-kB, and must be degraded prior to NF-kB activation. Our data show that doxorubicin exposure in MDA-MB-453 and MCF7 cells increases NF-kB activation (i.e. induces IKB degradation). In contrast, NF-kB was not modulated by any drug in BT-20 cells. NF-kB dependent autophagy is thought to be a pro-survival response (i.e. may be inhibiting chemotherapy). Furthermore, although pro-death autophagic responses are not well understood, they have been reported in various contexts. Thus, although autophagy was induced in all cell lines, the differential activation of NF-kB signaling may imply that these cell lines are using autophagy to

modulate survival in different ways. This hypothesis will be further investigated in the coming award period. Furthermore, STAT3 activation also suggested a difference between BT-20 cells and the other cells measured. STAT3 was robustly activated by doxorubicin in BT-20, but was not activated in any condition in the other cell lines. Finally, and potentially most interestingly, the DAPKs also revealed unique responses in BT-20 cells. Although DAPK2 was not activated DAPK1 was robustly activated in BT-20 cells. In addition, the activation was only seen in the ERL→DOX treatment condition in BT-20 cells, similar to what was seen for caspase-8. Thus, future modeling and future experimentation will also focus on the role for DAPK1 in the life/death decisions of TNBC cells.

Task 5. Determine activation of a subset of targets using multiplex *in vitro* kinase assays

In our proposal, we speculated that some data would need to be collected using *in vitro* kinase assays. These data are summarized in Figure 15. Reverse phase protein arrays and high-throughput Western blots both require the existence of high-fidelity antibodies, which simply do not exist for many of our targets of interest. One particularly important example is MAPKAPK2 (MK2). Our lab previous found that MK2 was critically important for DNA damage checkpoint signaling (Reinhardt et al., 2007). Furthermore MK2 was only found to be critical in p53-deficient cells, making MK2 a potentially cancer cell specific drug target. *In vitro* kinase assays were performed using kinase specific probes (Shults and Imperiali, 2003). *In vitro* kinase activity measurements were made for 5 kinases for probes currently exist: MEF2, ERK, AKT,

PKA, and MK2. Of these, ERK and AKT were also measured using other methods, so the activity measurements made here could be compared. Data collected for ERK and AKT was very similar to that collected using RPMA (Figure 15). Specifically, activity was decreased by erlotinib exposure. MEF2 was not activated by any of the conditions in our assay. PKA activity was increased by doxorubicin, decreased by erlotinib, and increased by the erlotinib/doxorubicin combinations, regardless of the timing of drug delivery. These data suggest that PKA responds to DNA damage, regardless of the presence or absence of EGFR signaling. Thus, differential modulation of PKA is not likely to play a role in the enhanced efficacy seen in BT-20 cells following the ERL→DOX treatment. Finally, MK2 activity was increased by doxorubicin exposure as well as exposure to the DOX/ERL treatment condition. MK2 activity was unchanged following erlotinib exposure and the ERL→DOX treatment condition. These data confirm our previous observations that MK2 responds to DNA damage signaling, but is inhibited by EGFR inhibition. Furthermore, this inhibitory effect did depend on the order and timing of EGFR inhibition, thus, loss of MK2 signaling may play a role in the enhanced chemosensitivity that we observed.

KEY RESEARCH ACCOMPLISHMENTS

- Identified a subset of signals within ErbB, DDR, cell cycle, apoptotic, and autophagic, metabolic networks that may contribute to the enhanced doxorubicin sensitivity observed in the ERL→DOX treatment condition.
- Collected a dataset to be used in mathematical modeling of the integrated DNA damage/EGFR signaling network in TNBC.
- Identified and confirmed an unexpected role for caspase-8 in mediating DNA damage responses.

REPORTABLE OUTCOMES

- Manuscript published in *Cell* (May 2012)
- Manuscript in preparation
- Invited to speak at *Gordon-Kenan Research Seminar on Phosphorylation and G Protein Mediated Signaling Networks: Novel Mechanisms and Therapeutic Approaches in GPCR and Kinase Signaling* (Biddeford, ME)
- Gene expression dataset submitted to Gene Expression Omnibus (GSE 30516)
- Applying to faculty positions to begin in September 2013
 - Research program focused on understanding TNBC heterogeneity and creating better therapeutic options of patients with TNBC

CONCLUSION

Triple-negative breast cancer continues to be a poorly understood form of cancer. In the first stage of this study, we performed a drug screen to identify combinations that were effective in killing TNBC cells. We identified that erlotinib (and EGFR inhibitor) could sensitize cells to doxorubicin (a DNA damaging agent) if—and only if—erlotinib was given at least 4 hours before doxorubicin. This striking time-dependent efficacy was unprecedented and is the focus of this award. Furthermore, this effect was only seen in TNBC cells. In this stage of the study, we were focused on 1) identifying changes induced by long-term exposure to erlotinib that could account for the increased chemosensitivity; 2) determining why this was unique to TNBC cells (and what does this tell us about TNBC); and 3) collecting a quantitative protein signaling dataset to be used for mathematical modeling. Our large scale signaling analyses identified a number of proteins that could be involved in the time-dependent efficacy we observed. Notable among these is caspase-8, an initiator caspase responsible for death receptor mediated apoptosis. Our findings reveal that DNA damage can, in some cases, utilize caspase-8 to enhance the cell death response. This response only happened in TNBC cells treated with erlotinib, and suggests a unique role played by EGFR signaling in the biology of TNBC. This point has been recently validated by a number of publications, in addition ours (Lee et al., 2012). Specifically, PTPN12, a phosphatase downstream of EGFR, was recently found to drive tumorigenesis in TNBC (Sun et al., 2011), and MEK inhibition (a protein downstream of EGFR) resulted in kinome reprogramming in TNBC (Duncan et al., 2012), similar to the genetic rewiring that we observed. These findings have collectively

further validated our claim that a subset of TNBC cells are driven by EGFR signaling. Finally, the dataset we collected appears to have the complexity and richness required to build data-driven models for computational analyses, as dictated in the statement of work. Thus, the future portions of this work can be completed as proposed.

Collectively, these data should have impact on: 1) the way we think about combination therapy, and 2) the way we treat triple-negative breast cancer. Our finding of time-dependent drug synergy and dynamic re-wiring of genetic networks provides a new model for testing and screening drug combinations, by taking advantage of (rather than ignoring) the compensatory mechanisms a cell uses when exposes to a drug. This finding has been received with great enthusiasm, even being called “arguably one of the first examples of systems biology really making a difference in translational research and beyond” (Erler and Linding, 2012). Secondly, the drug combination we identified appears to have efficacy in TNBC cells. In the future, we are interested in identifying how large of a patient population would be expected to receive benefit from this treatment, and testing this combination in the clinical setting.

References

- Albeck, J.G., Burke, J.M., Spencer, S.L., Lauffenburger, D.A., and Sorger, P.K. (2008). Modeling a snap-action, variable-delay switch controlling extrinsic cell death. *Plos Biol* 6, e299.
- Bosch, A., Eroles, P., Zaragoza, R., Viña, J.R., and Lluch, A. (2010). Triple-negative breast cancer: Molecular features, pathogenesis, treatment and current lines of research. *Cancer Treatment Reviews* 36, 206–215.
- Dancey, J.E., Bedard, P.L., Onetto, N., and Hudson, T.J. (2012). The Genetic Basis for Cancer Treatment Decisions. *Cell* 148, 409–420.
- Duncan, J.S., Whittle, M.C., Nakamura, K., Abell, A.N., Midland, A.A., Zawistowski, J.S., Johnson, N.L., Granger, D.A., Jordan, N.V., Darr, D.B., et al. (2012). Dynamic reprogramming of the kinome in response to targeted MEK inhibition in triple-negative breast cancer. *Cell* 149, 307–321.
- Erler, J.T., and Linding, R. (2012). Network Medicine Strikes a Blow against Breast Cancer. *Cell* 149, 731–733.
- Galluzzi, L., Vitale, I., Abrams, J.M., Alnemri, E.S., Baehrecke, E.H., Blagosklonny, M.V., Dawson, T.M., Dawson, V.L., El-Deiry, W.S., Fulda, S., et al. (2011). Molecular definitions of cell death subroutines: recommendations of the Nomenclature Committee on Cell Death 2012. *19*, 107–120.
- Green, D.R., and Evan, G.I. (2002). A matter of life and death. *Cancer Cell* 1, 19–30.
- Hanahan, D., and Weinberg, R.A. (2011). Hallmarks of Cancer: The Next Generation. *Cell* 144, 646–674.
- Harper, J.W., and Elledge, S.J. (2007). The DNA damage response: ten years after. *Mol Cell* 28, 739–745.
- Jin, S., and White, E. (2007). Role of autophagy in cancer: management of metabolic stress. *Autophagy* 3, 28–31.
- Lee, M.J., Ye, A.S., Gardino, A.K., Heijink, A.M., Sorger, P.K., Macbeath, G., and Yaffe, M.B. (2012). Sequential application of anticancer drugs enhances cell death by rewiring apoptotic signaling networks. *Cell* 149, 780–794.
- Levine, B. (2005). Autophagy in cell death: an innocent convict? *J Clin Invest* 115, 2679–2688.
- Mizushima, N., Yoshimori, T., and Levine, B. (2010). Methods in mammalian autophagy research. *Cell* 140, 313–326.
- Reinhardt, H.C., Aslanian, A.S., Lees, J.A., and Yaffe, M.B. (2007). p53-deficient cells

rely on ATM- and ATR-mediated checkpoint signaling through the p38MAPK/MK2 pathway for survival after DNA damage. *Cancer Cell* 11, 175–189.

Shults, M.D., and Imperiali, B. (2003). Versatile fluorescence probes of protein kinase activity. *J. Am. Chem. Soc.* 125, 14248–14249.

Subramanian, A., Tamayo, P., Mootha, V.K., Mukherjee, S., Ebert, B.L., Gillette, M.A., Paulovich, A., Pomeroy, S.L., Golub, T.R., Lander, E.S., et al. (2005). Gene set enrichment analysis: a knowledge-based approach for interpreting genome-wide expression profiles. *Proc Natl Acad Sci USA* 102, 15545–15550.

Sun, T., Aceto, N., Meerbrey, K.L., Kessler, J.D., Zhou, C., Migliaccio, I., Nguyen, D.X., Pavlova, N.N., Botero, M., Huang, J., et al. (2011). Activation of multiple proto-oncogenic tyrosine kinases in breast cancer via loss of the PTPN12 phosphatase. *Cell* 144, 703–718.

Tamayo, P., Steinhardt, G., Liberzon, A., and Mesirov, J.P. (2011). Gene Set Enrichment Analysis Made Right. 1–18.

Tentner, A.R., Lee, M.J., Ostheimer, G.J., Samson, L.D., Lauffenburger, D.A., and Yaffe, M.B. (2012). Combined experimental and computational analysis of DNA damage signaling reveals context-dependent roles for Erk in apoptosis and G1/S arrest after genotoxic stress. *Mol Syst Biol* 8, 568.

Zinkel, S.S., Hurov, K.E., Ong, C., Abtahi, F.M., Gross, A., and Korsmeyer, S.J. (2005). A role for proapoptotic BID in the DNA-damage response. *Cell* 122, 579–591.

Sequential Application of Anticancer Drugs Enhances Cell Death by Rewiring Apoptotic Signaling Networks

Michael J. Lee,^{1,2} Albert S. Ye,^{2,3} Alexandra K. Gardino,^{1,2} Anne Margriet Heijink,¹ Peter K. Sorger,^{2,4} Gavin MacBeath,^{2,4} and Michael B. Yaffe^{1,2,*}

¹Departments of Biology and Biological Engineering, David H. Koch Institute for Integrative Cancer Research

²Cell Decision Processes Center

Massachusetts Institute of Technology, Cambridge, MA 02139, USA

³Department of Molecular and Cellular Biology, Harvard University, Cambridge, MA 02138, USA

⁴Department of Systems Biology, Harvard Medical School, Boston, MA 02115, USA

*Correspondence: myaffe@mit.edu

DOI 10.1016/j.cell.2012.03.031

SUMMARY

Crosstalk and complexity within signaling pathways and their perturbation by oncogenes limit component-by-component approaches to understanding human disease. Network analysis of how normal and oncogenic signaling can be rewired by drugs may provide opportunities to target tumors with high specificity and efficacy. Using targeted inhibition of oncogenic signaling pathways, combined with DNA-damaging chemotherapy, we report that time-staggered EGFR inhibition, but not simultaneous coadministration, dramatically sensitizes a subset of triple-negative breast cancer cells to genotoxic drugs. Systems-level analysis—using high-density time-dependent measurements of signaling networks, gene expression profiles, and cell phenotypic responses in combination with mathematical modeling—revealed an approach for altering the intrinsic state of the cell through dynamic rewiring of oncogenic signaling pathways. This process converts these cells to a less tumorigenic state that is more susceptible to DNA damage-induced cell death by reactivation of an extrinsic apoptotic pathway whose function is suppressed in the oncogene-addicted state.

INTRODUCTION

Standard therapies for the treatment of human malignancies typically involve the use of chemotherapy or radiation therapy, which function by damaging DNA in both normal and cancerous cells (Lichter and Lawrence, 1995). Our growing understanding of this process suggests that the DNA damage response (DDR) functions as part of a complex network controlling many cellular functions, including cell cycle, DNA repair, and various forms of

cell death (Harper and Elledge, 2007). The DDR is highly interconnected with other progrowth and prodeath signaling networks, which function together to control cell fate in a nonlinear fashion due to multiple levels of feedback and cross-talk. Thus, it is difficult to predict a priori how multiple, often conflicting signals will be processed by the cell, particularly by malignant cells in which regulatory networks often exist in atypical forms. Predicting the efficacy of treatment and the optimal design of combination therapy will require a detailed understanding of how the DDR and other molecular signals are integrated and processed, how processing is altered by genetic perturbations commonly found in tumors, and how networks can be “rewired” using drugs individually and in combination (Sachs et al., 2005).

In many forms of breast cancer, aberrant hormonal and/or growth factor signaling play key roles in both tumor induction and resistance to treatment (Hanahan and Weinberg, 2000). Moreover, the identification of molecular drivers in specific breast cancer subtypes has led to the development of more efficacious forms of targeted therapy (Schechter et al., 1984; Slamon et al., 1987). In spite of these advances, there are currently no targeted therapies and no established molecular etiologies for triple-negative breast cancers (TNBC), which are a heterogeneous mix of breast cancers defined only by the absence of estrogen receptor (ER) or progesterone receptor (PR) expression and lack of amplification of the HER2 oncogene (Perou et al., 2000). Patients with TNBCs have shorter relapse-free survival and a worse overall prognosis than other breast cancer patients; however, they tend to respond, at least initially, to genotoxic chemotherapy (Dent et al., 2007). Triple-negative patients generally do well if pathologic complete response is achieved following chemotherapy. When residual disease exists, however, the prognosis is typically worse than for other breast cancer subtypes (Abeloff et al., 2008). Thus, identifying new strategies to enhance the initial chemosensitivity of TNBC cells may have substantial therapeutic benefit. We wondered whether a systems biology approach, focused on examining and manipulating the interface between growth factor signaling pathways and DNA damage signaling pathways in tumor cells, could

modulate the therapeutic response of this recalcitrant tumor type. We report here that pretreatment, but not cotreatment or posttreatment, of a subset of TNBCs with Epidermal Growth Factor Receptor (EGFR) inhibitors can markedly synergize their apoptotic response to DNA-damaging chemotherapy through dynamic rewiring of oncogenic signaling networks and unmasking of suppressed proapoptotic pathways. These results may have broader implications for the testing, design, and utilization of combination therapies in the treatment of malignant disease.

RESULTS

A Critical Order and Time Dependency for Enhanced EGFR Inhibition/DNA Damage-Mediated Cell Death

Signaling networks can respond to, and can be functionally rewired by, exposure to specific ligands or drugs (Janes et al., 2005, 2008). It is increasingly clear that these responses are time dependent. We reasoned that it should, in principle, be possible to dynamically rewire the DDR network in an insensitive cell through prior exposure to a drug that modulates the network, thereby rendering the cell sensitive to DNA-damaging agents. To test this hypothesis, we systematically investigated a series of drug combinations for synergism or antagonism in breast cancer cells using protocols that changed both the order and timing of drug addition.

We combined genotoxic agents with small molecule inhibitors targeting common oncogenic signaling pathways (Figure 1A). We included drugs that are known to be clinically useful in other cancers but are known to lack efficacy in TNBC individually or in combination (Bosch et al., 2010; Winer and Mayer, 2007). Previous studies using cell culture models of TNBC, for example, reported that EGFR inhibitors in combination with genotoxic compounds such as cisplatin resulted in less than a 10% survival benefit (Corkery et al., 2009), whereas a randomized phase II trial in TNBC patients reported that addition of cetuximab to carboplatin did not improve outcome (Carey et al., 2008). However, emerging understanding of the complex nonlinear and time-dependent interplay between signaling networks argues that a more systematic assessment exploring not only dosage, but also the order of drug presentation, scheduling, and dose duration might uncover cross-pathway effects and efficacious interactions that were missed previously (Fitzgerald et al., 2006). An initial combination screen was therefore performed in a panel of canonical breast cancer cell lines representing those that are hormone sensitive (MCF7), HER2 overexpressing (MDA-MB-453), or triple negative (BT-20) (Neve et al., 2006). A first pass of the screen, scoring for viability, was performed in BT-20 cells, and a subset of combinations was then explored more thoroughly, scoring for viability, proliferation, and apoptotic responses in the panel of three cell lines (Figures 1B–1E and Figure S1 available online).

Consistent with previous reports, we found that inhibition of EGFR using the compound erlotinib (ERL) was not a potent apoptotic stimulus in TNBC cells when used alone or when added at the same time as or shortly before doxorubicin (DOX) (Figure 1B, left bars 1–6). Surprisingly, however, combinations in which erlotinib was added at least 4 hr prior to doxorubicin showed a markedly enhanced apoptotic response, with cell

killing increasing by as much as 500% (Figure 1B, middle bars 7–10). When the order of drug presentation was reversed—doxorubicin given before erlotinib—cell killing was not enhanced relative to treatment with doxorubicin or erlotinib alone (Figure 1B, right bars 11 and 12). The efficacy of the time-sequenced erlotinib-doxorubicin treatment was analyzed for doxorubicin dose-effect relationships using the Chou-Talalay method (Chou and Talalay, 1984) and was found to vary significantly across breast cancer subtypes (Figures 1C–1E and 1G). Whereas chronic EGFR inhibition was synergistic with doxorubicin in killing TNBC BT-20 cells, the same treatment regimen antagonized doxorubicin sensitivity in HER2-overexpressing MDA-MB-453 cells. All temporal erlotinib-doxorubicin combinations tested were merely additive in luminal MCF7 cells. The order and timing of drug addition had little effect in Hs578Bst, a cell line derived from normal peripheral breast tissue, which was generally drug resistant (Figure 1F).

Furthermore, this enhanced treatment effect in BT-20 cells was not limited to combinations of doxorubicin and erlotinib. Synergistic killing was also observed following time-staggered pretreatment of BT-20 cells with either erlotinib, gefitinib, or lapatinib (all EGFR inhibitors) in combination with the DNA-damaging agent camptothecin, as well as with doxorubicin (Figures S1A–S1C) (Wood et al., 2004).

Sustained EGFR Inhibition Suppresses Oncogenic Signatures and Rewires the Intrinsic State of the Tumor Cells to a More Chemosensitive Form

Although erlotinib inhibits EGFR and downstream signaling within minutes (Figures S2A and S2B), enhanced cell death in response to DNA-damaging agents required pretreatment with erlotinib for several hours. To verify that this was indeed due to on-target inhibition of EGFR, in addition to testing other EGFR inhibitors (above), we knocked down EGFR using two different small interfering RNAs (siRNAs). Like the time-staggered erlotinib-doxorubicin treatment, strong proapoptotic responses were observed in BT-20 cells following EGFR knockdown with delayed doxorubicin treatment (Figures 1H and 1I). Importantly, the addition of erlotinib to EGFR knockdown cells had no additional effect, arguing against an off-target effect of the drug. As a further test, we also examined coadministration of higher concentrations of erlotinib instead of time-staggered doses without observing increased apoptosis (Figure S2C). Taken together, these data indicate that enhanced cell death observed using time-staggered erlotinib-doxorubicin combinations is directly mediated by sustained EGFR inhibition.

Potential explanations for the increased sensitivity of cells to doxorubicin following sustained EGFR inhibition include modulation of cell-cycle progression, altered rates of doxorubicin influx/efflux, or changes in levels of DNA damage itself. To examine these, we monitored cell-cycle progression at five time points over 24 hr in our panel of breast cancer cell lines. Although doxorubicin and erlotinib altered cell-cycle dynamics depending on the cell type, cells that received both drugs had similar cell-cycle profiles regardless of the dosing regimen (Figures 2A–2D and S2D). In particular, there is no evidence that cells exposed to the ERL→DOX protocol accumulate in S/G2, the cell-cycle stage during which doxorubicin may be most effective. Thus,

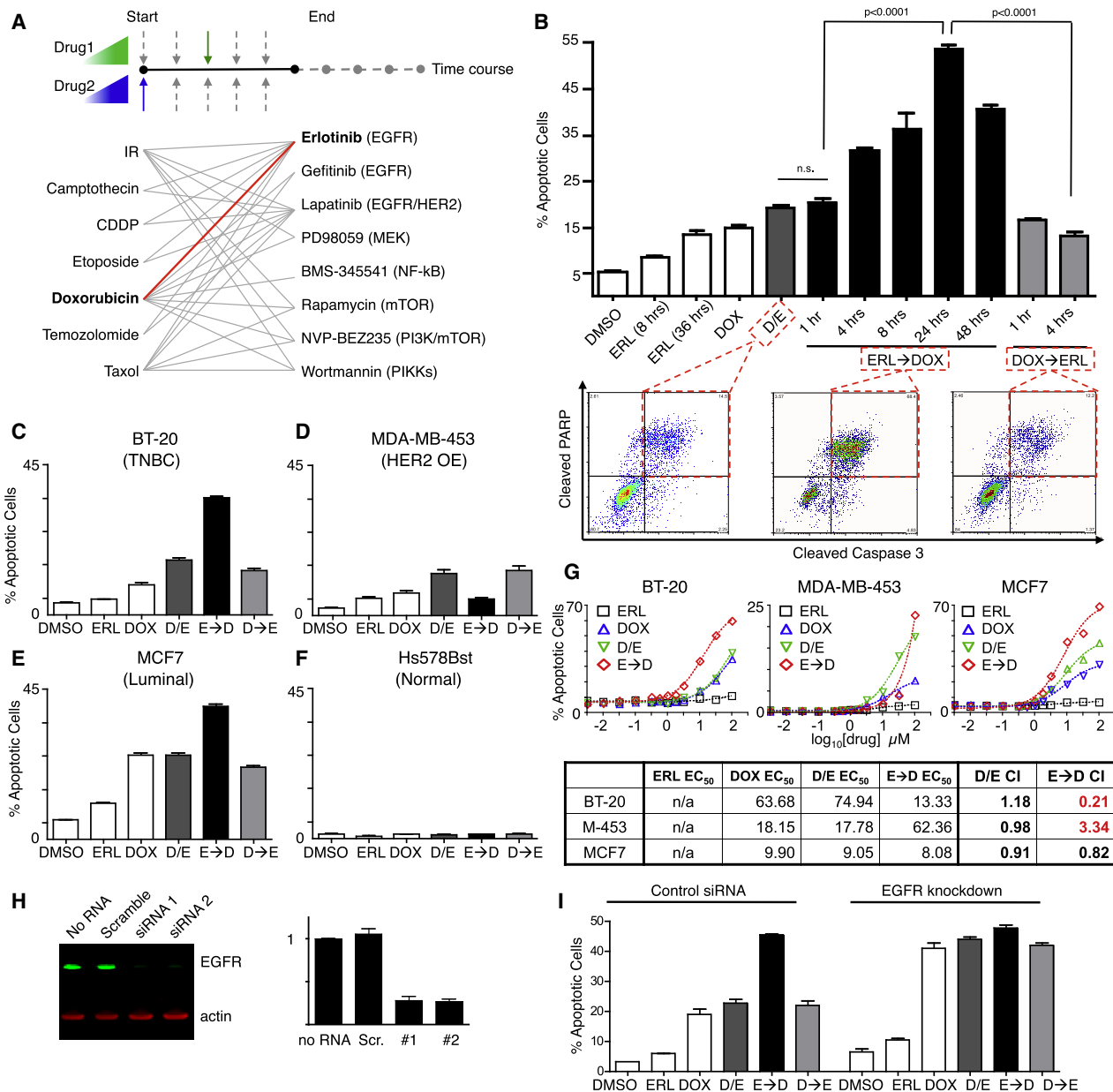


Figure 1. A Screen for Novel Combination Treatment Reveals Dosing Schedule-Dependent Efficacy for Killing TNBC Cells

(A) Schematic of combinations tested. Seven genotoxic drugs and eight targeted signaling inhibitors were tested in pair-wise combinations, varying dose, order of presentation, dose duration, and dosing schedule.

(B) Apoptosis in BT-20 cells. Cleaved-caspase 3/cleaved-PARP double-positive cells were quantified using flow cytometry (bottom). In cells treated with DMSO, erlotinib (ERL), or doxorubicin (DOX), apoptosis measurements were performed 8 hr after drug exposure or at the indicated times. D/E, ERL → DOX, and DOX → ERL refer to DOX and ERL added at the same time, ERL given at the indicated times before DOX, and DOX given at the indicated times before ERL, respectively. For each, apoptotic measurements were made 8 hr after the addition of DOX. Erlotinib and doxorubicin were used at 10 μM. Mean values ±SD of three independent experiments, each performed in duplicate, are shown (top).

(C–F) Apoptosis in different subtypes of breast cancer. Apoptosis was measured as in (B). (D and E) E → D and D → E refer to DOX and ERL added at the same time, ERL given 24 hr before DOX, and DOX given 4 hr before ERL, respectively. Data are mean values ±SD of three independent experiments.

(G) Dose-response profiles of erlotinib/doxorubicin drug combinations. Apoptosis was measured as in (B). Drugs were added at a 1:1 ratio, and combination index (CI) was calculated according to the Chou-Talalay method.

(H) Knockdown of EGFR in BT-20 cells measured 48 hr after addition of the indicated siRNA by immunoblotting (left). EGFR expression relative to “no RNA” control is quantified on right.

(I) Apoptosis in BT-20 cells ± EGFR knockdown measured as in (B). Scrambled RNAi shown as control. Data shown are the mean ±SD of both siRNAs, each performed in biological duplicate.

See also Figure S1.

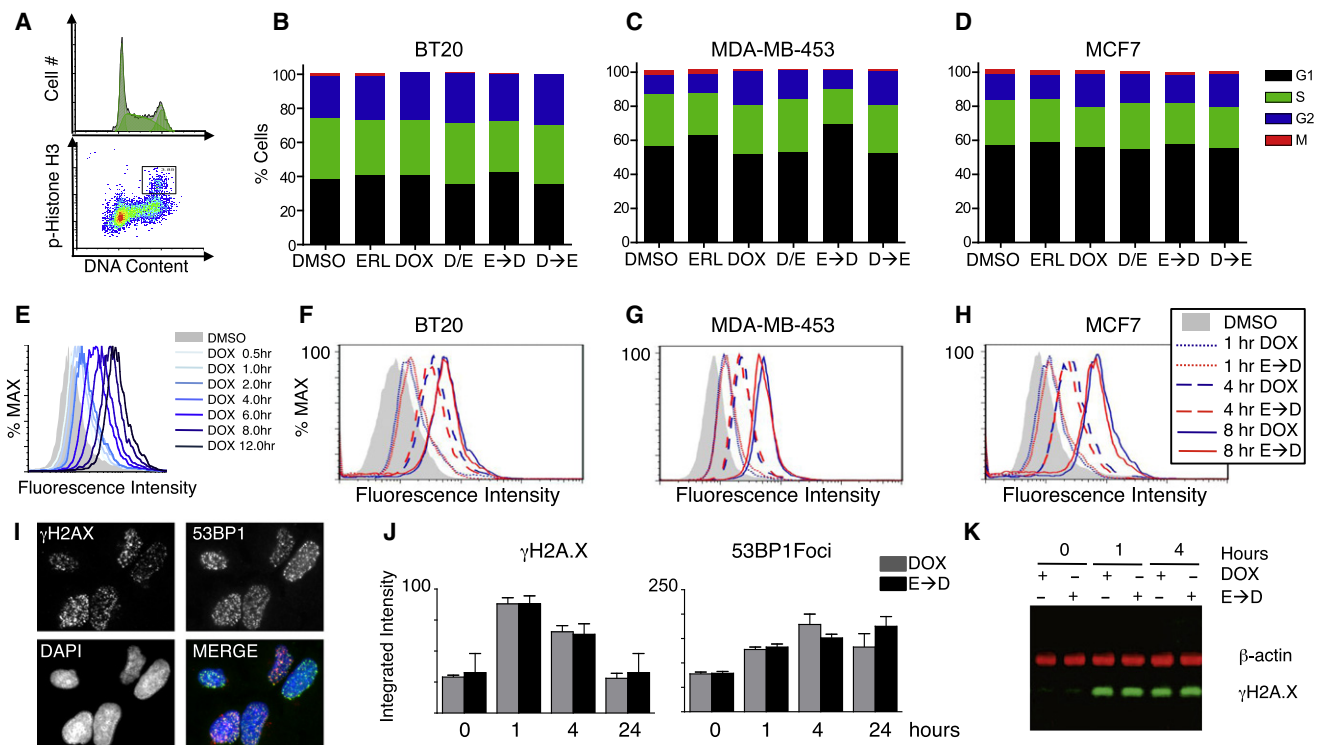


Figure 2. Prolonged Treatment with Erlotinib Does Not Change Cell-Cycle Profile, Doxorubicin Influx/Efflux, or the Level of DNA Damage
 (A–D) Quantitative cell-cycle analysis. DNA content and the percentage of mitotic cells were measured by FACS. (A) Example FACS plots from untreated BT-20 cells. (B–D) Cell-cycle stage quantified from three experiments, each performed in duplicate. Cells were treated as in Figure 1, and data were collected at 6, 8, 12, 24, and 48 hr after DOX treatment. 8 hr data shown for each cell type.
 (E–H) Doxorubicin retention measured by flow cytometry. (E) Sample time course of BT-20 cells treated with 10 μ M DOX for the indicated times. (F–H) Cells treated with doxorubicin or pretreated with erlotinib for 24 hr prior to DOX (E \rightarrow D). Cells were collected at 1, 4, or 8 hr after DOX exposure as indicated, and internal doxorubicin fluorescence was measured.
 (I and J) Quantitative microscopy of the early DNA double-stranded break response. (I) Example image of cells treated with DOX for 1 hr and stained for γ H2AX, 53BP1, or nuclear content (DAPI). (J) Integrated intensity per nucleus of γ H2AX and 53BP1 foci was measured in BT-20 cells after the indicated treatments and times. Mean values \pm SD from triplicate experiments shown.
 (K) Western blot analysis of γ H2AX in BT-20 cells. β -actin shown as a loading control.
 See also Figure S2.

cell-cycle modulation cannot explain the unique efficacy of sequential drug exposure. Some membrane pumps can be modulated by EGFR inhibitors (Lopez et al., 2007; Turner et al., 2006) and are responsible for multidrug resistance in at least some breast cancers (Woehlecke et al., 2003). We therefore measured the intracellular accumulation of doxorubicin by flow cytometry and found that prior treatment with erlotinib did not alter the intracellular doxorubicin concentration (Figures 2E–2H). Next, as pharmacodynamic markers of doxorubicin action, we assayed two indicators of DNA double-stranded breaks: phosphorylation of histone H2AX at S139 and formation of 53BP1-containing nuclear foci. Both assays showed similar responses across all treatment conditions (Figures 2I–2K). Taken together, these data indicate similar levels of DNA damage and early DNA damage-related signaling in DOX- and ERL \rightarrow DOX-treated cells independent of the efficacy of the combination in cell killing.

The absence of demonstrable changes in cell-cycle states, intracellular doxorubicin concentrations, or doxorubicin-induced

DNA damage suggested that prolonged EGFR inhibition necessary for effective tumor cell killing might result from rewiring of the signaling networks that control responses to genotoxic stress. To investigate this idea, we measured changes in gene expression in cells treated with erlotinib alone. In triple-negative BT-20 cells, EGFR inhibition for 30 min resulted in few differentially expressed genes (DEGs) (Figure S3A). Following 6 hr of erlotinib treatment, however, we observed >1,200 DEGs, and following 24 hr of treatment, when doxorubicin sensitivity was maximally enhanced, we observed >2,000 DEGs (Figures 3A and S3B). By comparison, in the HER2+ MDA-MB-453 cells, which were desensitized to doxorubicin by erlotinib exposure, we observed only 235 DEGs following 24 hr exposure to erlotinib, and in hormone-sensitive MCF7 cells, only one gene was significantly altered (Figures 3B and 3C). Thus, the triple-negative BT-20 cells exhibited progressive and large-scale changes in gene expression following EGFR inhibition that were not observed in cell lines insensitive to the time-staggered ERL \rightarrow DOX combination.

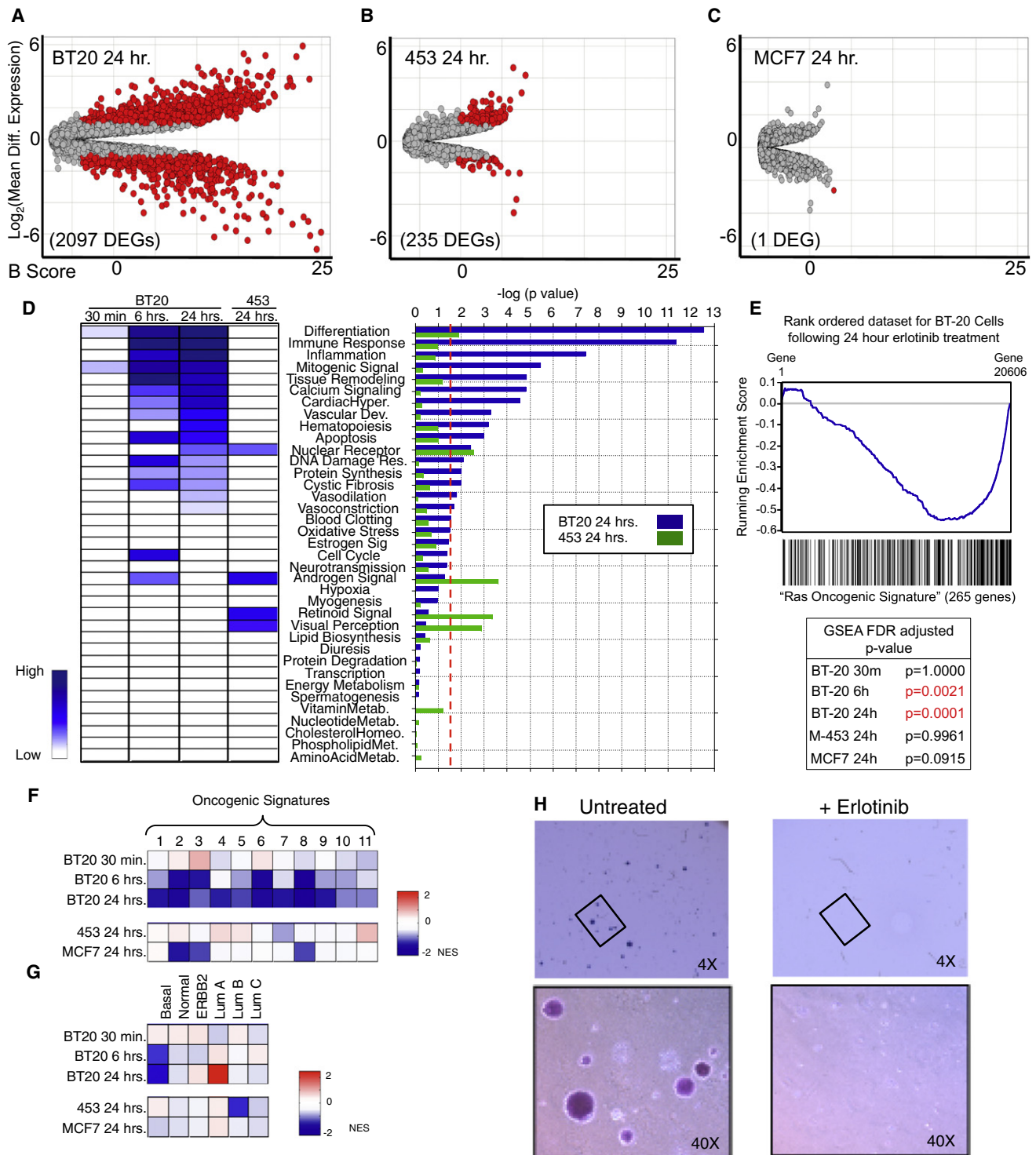


Figure 3. Triple-Negative BT-20 Cells Are Driven by Oncogenic EGFR Signaling

(A–C) DEGs following erlotinib treatment for 24 hr versus untreated cells. Cut-off for DEG was ≥ 2 -fold change and a p value ≤ 0.05 (genes that meet both criteria are colored red). B score is the log of the odds of differential expression.

(D) DEGs classified using GeneGO "pathway maps." Heatmap (left) colored according to $-\log(p \text{ value})$; (right) p value cut-off was 0.05 (dotted red line).

(E and F) Microarray analysis using GSEA reveals loss of oncogene signatures in BT-20 cells after sustained EGFR inhibition. Ras oncogenic signature and false discovery rate (FDR)-adjusted p values are shown in (E). Eleven oncogenic signatures from the Molecular Signatures Database (MSigDB) are shown in (F). Boxes are colored according to normalized enrichment score (NES).

To examine which cellular processes were altered by long-term erlotinib treatment, DEGs in BT-20 cells were categorized by cellular process according to the GeneGO pathway annotation software (Ekins et al., 2007). Significant changes were observed in 16 of 34 GeneGO cellular networks, including those that mediate the DDR, apoptosis, and inflammation (Figure 3D). In contrast, DEGs in MDA-MB-453 were not only fewer in number, but also lay in networks that did not overlap with those altered in BT-20 cells (Figure 3D). We further analyzed gene expression data using gene set enrichment analysis (GSEA), a tool for identification of enrichment or depletion of defined gene expression signatures within a rank-ordered gene list (Subramanian et al., 2005). The most statistically significant changes in BT-20 cells upon sustained erlotinib exposure were loss of the Ras and MYC oncogenic signatures (Figure 3E). These signatures were not significantly altered in MDA-MB-453 or MCF7 cells treated with erlotinib for 24 hr or in BT-20 cells exposed to erlotinib for 30 min (Figure 3E). Within the GSEA molecular signatures database, there exist 11 oncogenic signatures (Subramanian et al., 2005). GSEA of EGFR-inhibited BT-20 cells showed a similar depletion pattern for all 11 oncogenic signatures (Figure 3F). These changes were not consistently observed in either MDA-MB-453 cells or MCF7 cells following exposure to erlotinib.

Distinct gene expression patterns have been used to define breast cancer subtypes. BT-20 cells, like most triple-negative cells, display a “basal-like” gene expression signature (Neve et al., 2006). Strikingly, analysis of our expression data set revealed that chronic erlotinib treatment of BT-20 cells caused progressive time-dependent loss of basal-like gene expression with concomitant gain in luminal A-like gene expression, a breast cancer subtype with the least aggressiveness and best overall prognosis (Figure 3G). In contrast, no such switch in breast cancer subtype patterns of gene expression was observed in HER2-overexpressing MDA-MB-453 cells or hormone-sensitive MCF7 cells following erlotinib exposure.

These expression data suggest that the oncogenic potential of BT-20 cells is maintained by chronic EGFR-driven patterns of gene expression and that this cell state could be remodeled through sustained inhibition of EGFR. To directly test this, we examined the ability of BT-20 cells to form colonies in soft agar, a classic test of transformation that typically shows good correlation with tumorigenic potential in vivo (Montesano et al., 1977). Consistent with the predictions derived from our GSEA, sustained EGFR inhibition with erlotinib potently inhibited soft agar colony formation (Figure 3H).

Creation of a Data-Driven Model for Combined EGFR Inhibition/DNA Damage

To better understand the biochemical changes in signaling that accompany time-staggered ERL→DOX treatment, we used quantitative high-throughput reverse-phase protein microarrays

and quantitative western blotting to measure the levels or activation states of 35 signaling proteins within multiple signaling pathways at 12 time points following exposure to erlotinib and doxorubicin both individually and in combination (Figures 4A–4D and see Figure S4 for a description of the selection of 35 proteins for analysis) (MacBeath, 2002). Oncogenic signaling networks typically exhibit multiple levels of feedback and crosstalk with other networks, rendering single protein measurements ineffective in predicting complex cellular responses to drugs such as those leading to DNA damage-induced apoptosis (Fitzgerald et al., 2006). We therefore constructed a multifactorial data-driven mathematical model relating signaling “inputs” to phenotypic “outputs.” In addition to examining signaling pathways known to contribute to the DDR, we used our list of differentially expressed genes (Figure 3) to identify other proteins that might function as critical signaling nodes. This DEG-expanded list of signaling proteins extends far beyond the canonical components of the DDR, including proteins involved in apoptotic and nonapoptotic death, growth and stress responses, and cytokine/inflammatory signaling (Figure S4A). Specific proteins, whose measurement was motivated by gene expression data, included Bcl2-interacting mediator of cell death (BIM), BH3-interacting domain (BID), caspase-8, 4E-BP1, S6K, Stat3, DUSP6, and inhibitor of kappa B (IKB). Phenotypic responses, including cell-cycle arrest and progression, autophagy, and apoptotic and nonapoptotic cell death, were scored at six time points using luminescent microplate assays, flow cytometry, and automated microscopy (Figures 4E and S4C–S4F). All signaling and phenotypic response measurements were performed in biological and experimental triplicate in BT-20, MDA-MB-453, and MCF7 cells. In total, this data set comprised more than 45,000 measurements of molecular signals and 2,000 measurements of cellular responses (Figures 4A and 4E), revealing many changes in cell state and phenotype associated with drug exposure.

Several mathematical modeling approaches were employed to relate signaling data to cell phenotypes. Initial modeling efforts used principal component analysis (PCA) to identify covariation between signals, whereas partial least-squares (PLS) regression was used to identify statistically significant covariation between molecular signals and corresponding cellular responses (Figure S4B) (Janes and Yaffe, 2006). In both PCA and PLS modeling, vectors were constructed whose elements contained quantitative measures of the level, state, and/or activity of specific signaling proteins. The vectors were then reduced to a set of principal components, calculated so that each additional PCA or PLS dimension maximally captures information not captured by preceding components. This process was iteratively repeated until additional principal components ceased to capture meaningful data, as judged relative to experimental noise.

(G) GSEA reveals a switch from basal to luminal A genetic signature in BT-20 cells following sustained EGFR inhibition. Expression analyzed as in (F) using breast cancer subtype-specific genetic signatures as defined by Sorlie et al. (2001).

(H) BT-20 cells lose the ability to form colonies in soft agar upon EGFR inhibition. Cells were untreated or treated with ERL, grown in soft agar, and monitored for colony formation 21 days later.

See also Figure S3.

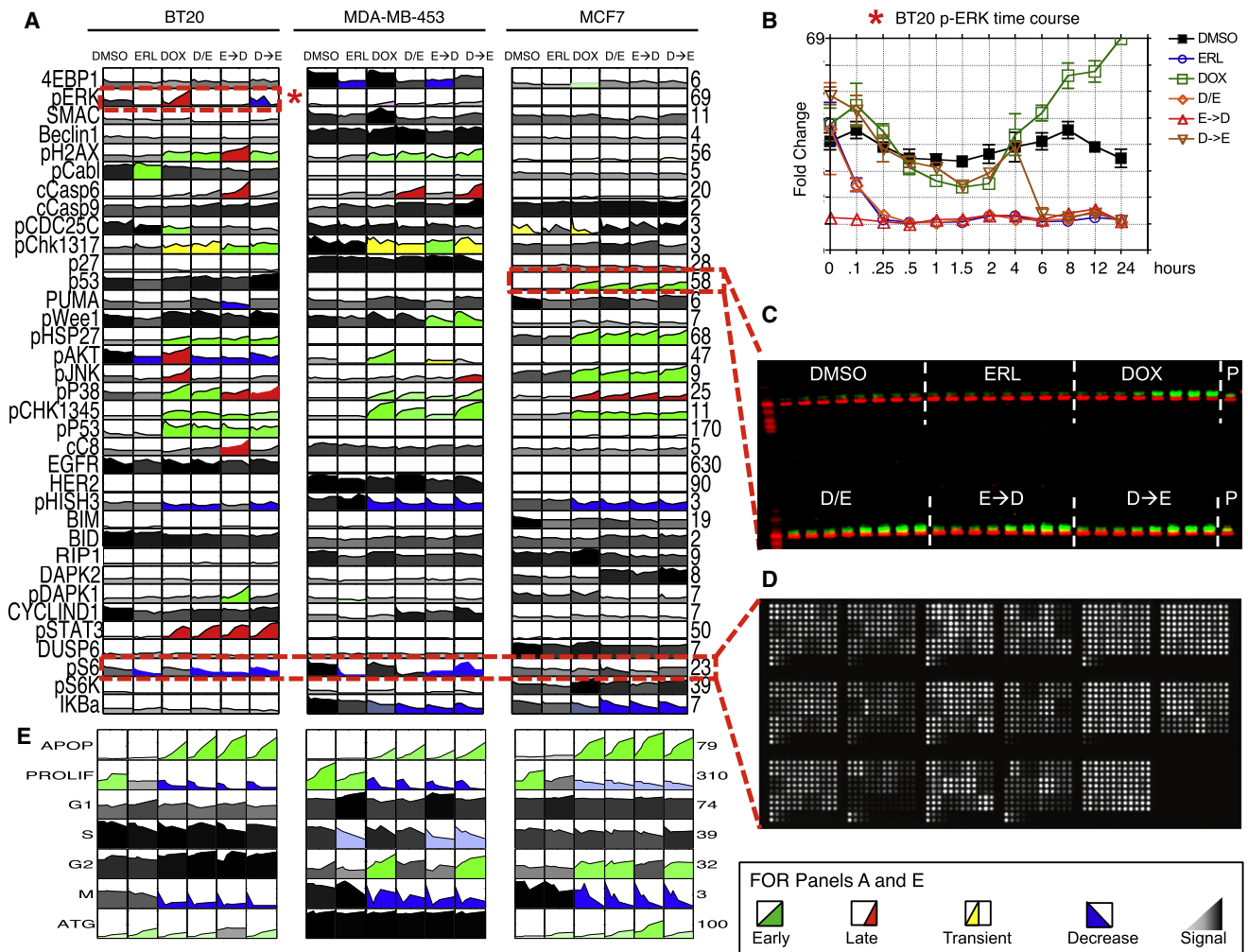


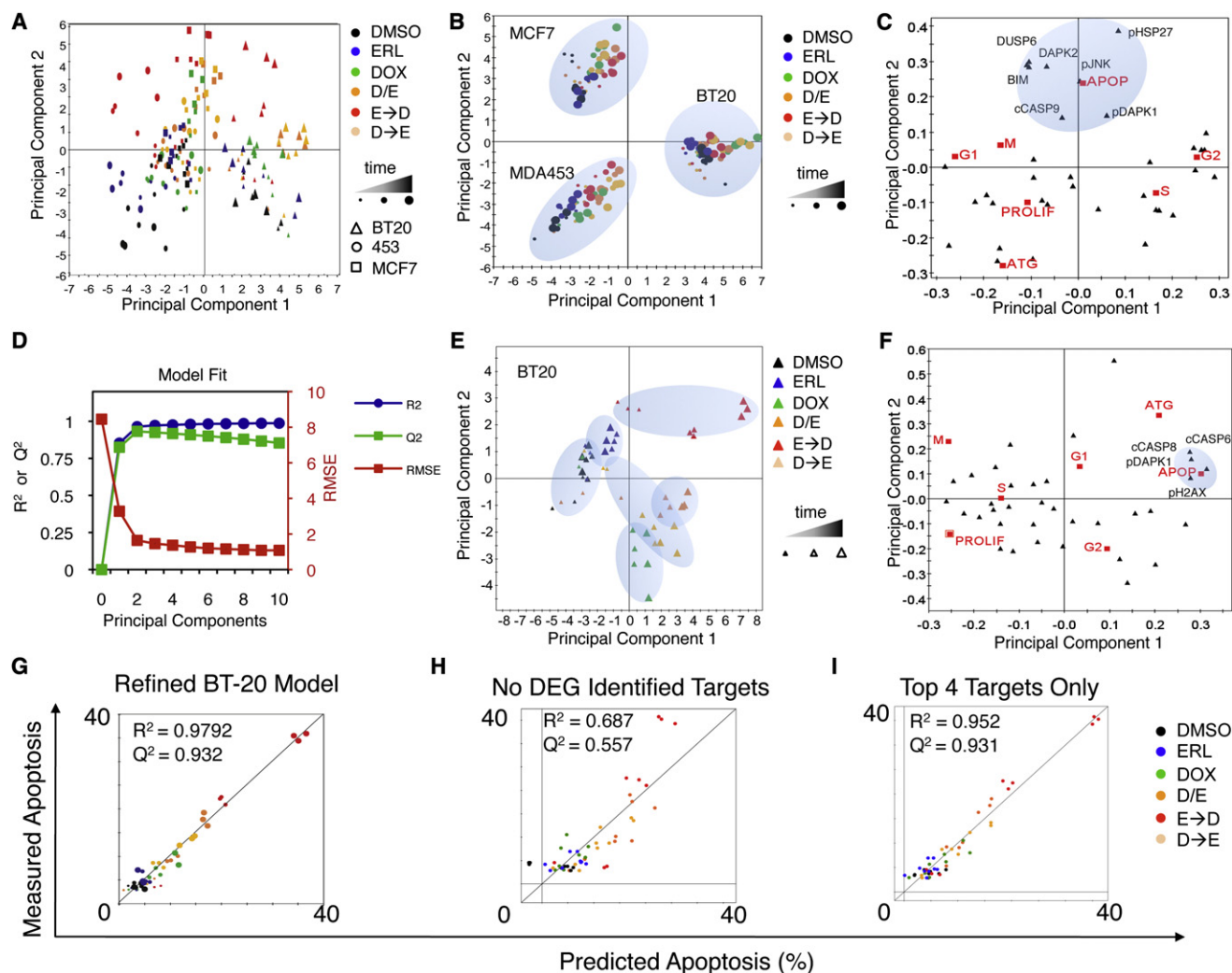
Figure 4. A Systems-Level Signal-Response Data Set Collected Using a Variety of High-Throughput Techniques

(A–D) (A) The complete signaling data set for three different breast cancer subtypes following combined EGFR inhibition and genotoxic chemotherapy treatments as in Figure 1. Each box represents an 8 or 12 point time course of biological triplicate experiments. Time course plots are colored by response profile, with early sustained increases in signal colored green, late sustained increases colored red, and transient increases colored yellow. Decreases in signal are colored blue. Signals that are not significantly changed by treatment are shaded gray to black with darkness reflecting signal strength. Numbers to the right of each plot report fold change across all conditions and/or cells. (B) Sample detailed signaling time course from (A), highlighted by dashed box and asterisk, showing p-ERK activation in BT-20 cells. Mean values \pm SD of three experiments are shown. (C) Forty-eight-sample western blots analyzed using two-color infrared detection. Each gel contained an antibody-specific positive control (P) for blot-to-blot normalization. The example shown is one of three gels for total p53 in MCF7 cells (p53 in green; β -actin in red). (D) Reverse-phase protein lysate microarrays were used to analyze targets of interest when array-compatible antibodies were available. The slide shown contains \sim 2,500 lysate spots (experimental and technical triplicates of all of our experimental samples, and control samples used for antibody calibration), probed for phospho-S6.

(E) The complete cellular response data set, colored as in (A). See also Figure S4 and Table S1.

Following PCA, multiplex data from MDA-MB-453 cells projected negatively along principal component one (PC1), data from BT-20 cells projected positively along PC1, and MCF7 data were largely neutral (Figures 5A and S5A). Thus, the first principal component captured cell type-specific variance in the data. In contrast, data from all cell types projected similarly along PC2 but in a manner that was drug dependent. Data from DMSO- or erlotinib-treated cells not exposed to doxorubicin projected negatively along PC2, whereas data from cells

cotreated with doxorubicin and erlotinib or exposed sequentially to ERL \rightarrow DOX projected positively along PC2. Finally, data from cells treated with doxorubicin alone or DOX \rightarrow ERL were largely neutral along PC2. Thus, the second principal component captured signaling variance from treatment-specific modulation of the signaling networks regardless of cell type (Figure 5A). These data suggest that, although significant differences in the state of the networks exist between cell lines, the drugs that we applied modulated signaling networks in similar ways across



model (Figure 5D), a common finding reflecting the addition of noise when components with little predictive value are added. Similar trends were observed for each of the other cell lines. To derive molecular understanding from the models, we projected the loading vectors (i.e., individual signals and responses) into PLS component space. We observed a strong anticorrelation between the apoptotic and proliferative responses (Figures 5C and 5F) that was captured by the first principal component in the BT-20 model (Figure 5F) and by the second principal component in the aggregate cell line model (Figure 5C). To further test model quality, we compared each measured cellular response in isolation to that predicted by the model using jack-knife-based cross-validation (Figures S5F–S5L). Our model was particularly accurate at predicting apoptosis following treatment (Figure 5G) and was moderately good at predicting proliferation and autophagy (Figures S5K and S5L). Other responses (G1, G2, and S) were not predicted as accurately, likely due to the limited dynamic range in our cell-cycle response data set (Figures S5G–S5J).

PLS Modeling Reveals that Chemosensitization following Network Rewiring Is Driven by Caspase-8 Activation

Because PLS models of individual cell lines could accurately predict apoptosis, we analyzed the models to identify specific proteins or signals that might account for the enhanced sensitivity of BT-20 cells to doxorubicin following EGFR inhibition. The BT-20 two-component PLS model identified four signals (cleaved caspase-8, cleaved-caspase-6, phospho-DAPK1, and phospho-H2AX) that were highly covariant with apoptosis (Figure 5F). Remarkably, a model including only these four signals was just as accurate at predicting apoptosis as the complete 35-signal model (Figures 5G–5I). Notably, of these signals, only pDAPK1 would have been identified using the aggregate cell line PLS model (Figure 5C). We reasoned that the enhanced sensitivity of BT-20 cells to doxorubicin, mediated by erlotinib pretreatment, likely involved one of these molecular signals. We therefore calculated and plotted the “variable importance in the projection” (VIP) score for each signal (Figure 6A). The VIP score reports the sum (over all model dimensions) of each variable x (molecular signals in this case), weighted by the amount of the cellular response y (apoptosis) explained by variable x . Strikingly, caspase-8, an initiator caspase in death receptor-mediated apoptosis, was the single most important variable for predicting apoptosis in BT-20 cells and was simultaneously among the least important variables in MDA-MB-453 and MCF7 cells. Caspase-8 has previously been implicated in cell death mediated by EGFR inhibition in other contexts (Kang et al., 2010; Morgillo et al., 2011); however, erlotinib alone did not cause death in any of our cell types. Instead, apoptosis in these cells and the potential importance of caspase-8 resulted from their exposure to the genotoxic agent doxorubicin. In most cells, DNA damage activates cell-intrinsic apoptosis mediated through caspase-9 (c.f., Figure 5C), not caspase-8 (Kim, 2005). Thus, the strong influence of caspase-8 was unexpected.

As an *in silico* test for the importance of caspase-8 in particular erlotinib/doxorubicin protocols, we set caspase-8 activity to zero in the model and left all other variables unchanged. The

BT-20 model specifically predicted a dramatic decrease in the enhanced sensitivity to doxorubicin following sustained erlotinib treatment (Figure 6B), with much smaller decreases in apoptosis occurring under all other treatments. In contrast, the apoptosis model for MDA-MB-453 cells predicted no change following loss of caspase-8 activity under any conditions (Figure 6C). To test these predictions experimentally, two separate caspase-8 siRNAs were used in both BT-20 cells and MDA-MB-453 cells (Figures 6D and 6E). In excellent agreement with the model, knockdown of caspase-8 mitigated the enhanced cell death following erlotinib treatment in BT-20 cells while having minimal effect on apoptosis following other treatment combinations (Figure 6F). Furthermore, caspase-8 knockdown had little effect on apoptosis in MDA-MB-453 under any condition (Figure 6G). To further assess model predictions and evaluate the relative importance of caspase-8 in the enhanced doxorubicin-induced apoptosis, we tested several other model-generated predictions, including proteins predicted to contribute strongly (caspase-6), moderately (Beclin-1), or weakly (RIP1) to apoptosis in BT-20 cells. Based on the VIP plot and loadings projections, caspase-6 is predicted to be a strong driver of the apoptotic response in BT-20 and MDA-MB-453 cells, but not MCF7 cells; Beclin-1 is predicted to be moderately antiapoptotic in BT-20 cells but has no role in the other cell lines; and RIP1 is predicted to be weakly antiapoptotic in BT-20 and MDA-MB-453 cells but strongly antiapoptotic in MCF7 cells. As shown in Figure S6, we were able to confirm these cell type dependences using siRNA and confirm the relative magnitude of the effect of each target on the apoptotic response following various combinations of erlotinib and/or doxorubicin. Importantly, although caspase-6 contributed strongly to cell death in BT-20 cells, caspase-8 remained the strongest predictor. None of the other targets tested modulated the apoptotic response to the same extent as caspase-8, further highlighting its importance. Thus, the increased cell killing by ERL→DOX treatment in BT-20 cells appears to involve rewiring of the DNA damage response, allowing activation of both cell-intrinsic and -extrinsic apoptotic programs to contribute to cell death.

Time-Staggered Inhibition of EGFR Enhances Apoptotic Response in a Subset of TNBC Cells and Other Oncogene-Driven Cells

To examine whether the efficacy of time-staggered ERL→DOX treatment was unique to BT-20 cells or potentially a more general phenomenon of TNBC cells, we examined a handful of other triple-negative cell lines (Neve et al., 2006). The selected cell lines have markedly different growth rates, EGFR expression levels, and p53 states (Figure S7A). Despite these differences, sustained EGFR inhibition enhanced sensitivity to doxorubicin in nine of ten triple-negative cell lines tested. A synergistic effect, however, was observed in only four of the ten TNBC lines (Figures 7A, S7A, and S7B). To identify potential reasons for this, we measured total EGFR protein levels and basal EGFR activation by immunoblotting. Our quantitative measurement of EGFR protein expression was very similar to previously reported values (Neve et al., 2006) and correlated only very weakly with sensitivity to ERL→DOX treatment (Figures 7A and 7B). In marked contrast, the levels of basal EGFR activity exhibited

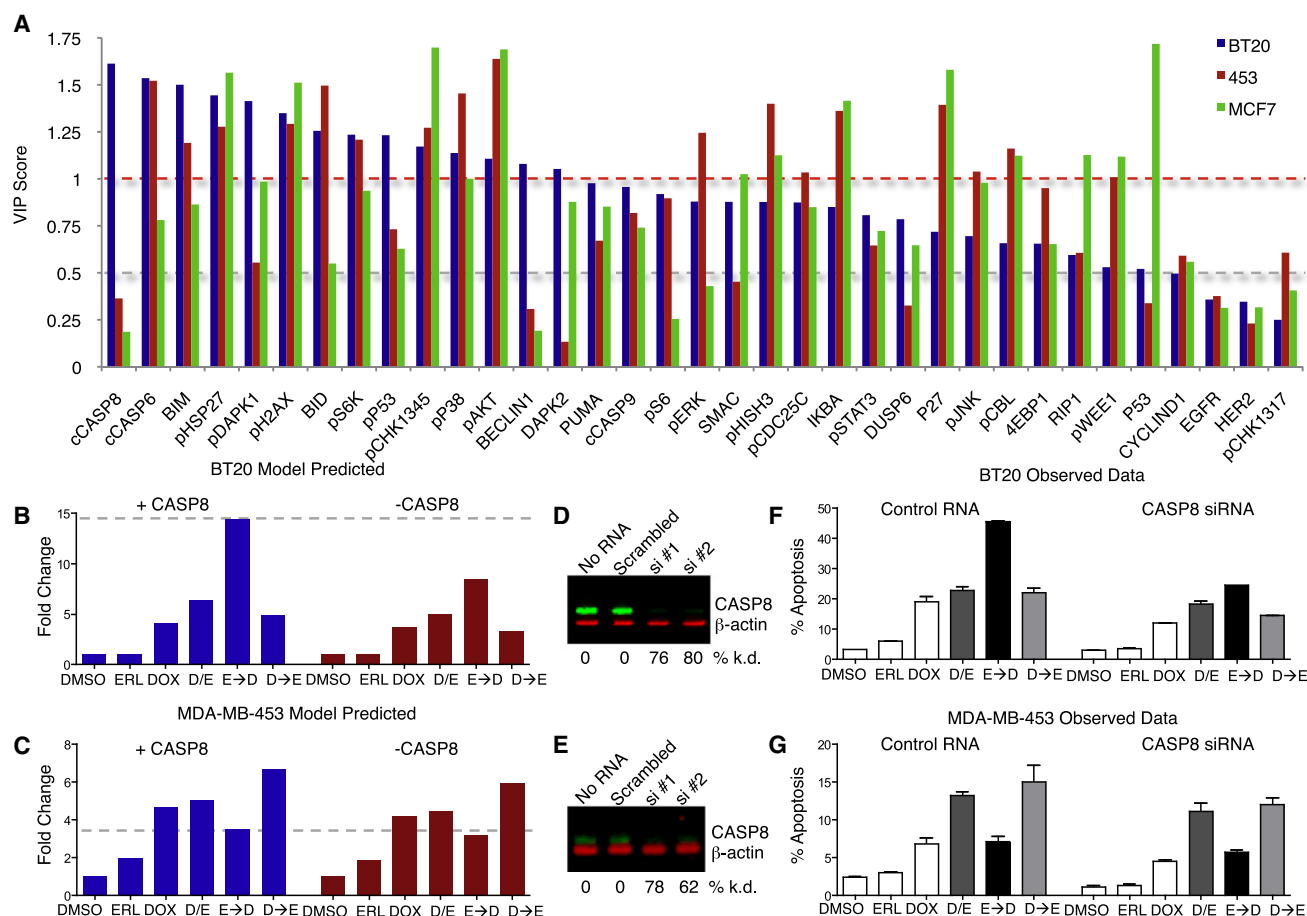


Figure 6. Enhanced Sensitivity to Doxorubicin Is Mediated by Caspase-8 Activation

(A) VIP scores for predicting apoptosis plotted for each cell line-specific PLS model. VIP score >1 indicates important x variables that predict y responses, whereas signals with VIP scores <0.5 indicate unimportant x variables.

(B and C) Model-generated predictions of apoptosis with (blue) or without (red) caspase-8 activation 8 hr after the indicated treatments in BT-20 (B) and 453 (C). (D and E) Western blot verifying caspase-8 knockdown in BT-20 (D) and 453 (E).

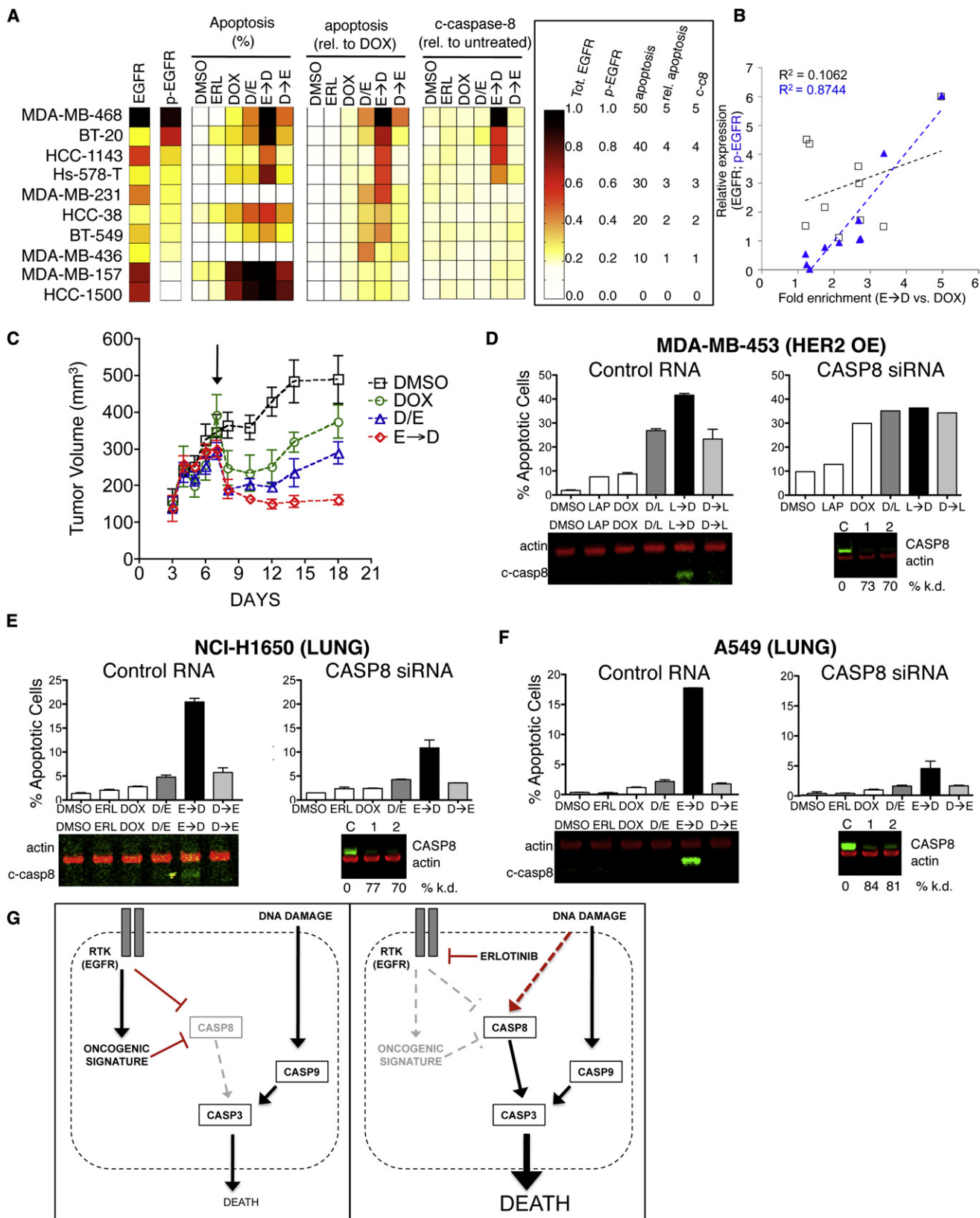
(F and G) Measured apoptosis 8 hr after the indicated treatment in cells expressing control RNA or caspase-8 siRNA. (F) BT-20. (G) 453. In both (F) and (G), apoptotic values represent mean response \pm SD from both siRNAs, each in duplicate.

See also Figure S6.

a much higher correlation (Figures 7A and 7B). Furthermore, in those TNBC cell lines in which ERL \rightarrow DOX treatment was synergistic, we consistently observed caspase-8 cleavage following sequential administration, but not other drug treatments, suggesting a similar mechanism of enhanced apoptosis in these cells as that observed in BT-20 cells (Figures 7A and 7B). Taken in context with our observation that EGFR signaling drives expression of an oncogenic gene expression signature in BT-20 cells, these findings suggest that a subset of triple-negative cell lines are similarly driven by aberrant EGFR signaling. Importantly, however, these cells could not be distinguished by measuring EGFR gene amplification or EGFR abundance. Instead, they are unique in displaying high levels of activated (phosphorylated) EGFR as a biomarker of response to time-staggered EGFR inhibition and cytotoxic treatment.

We next investigated whether the initial chemosensitizing effects of an ERL \rightarrow DOX protocol could be observed when treating EGFR-driven triple-negative tumors in vivo. BT-20 cells

were injected into the flanks of nude mice, and tumors were allowed to form for 7 days before treatment with either doxorubicin alone or erlotinib-doxorubicin combinations. Following a single dose of doxorubicin alone, a marked reduction in tumor volume was observed over the first 3 days after treatment. The residual tumors continued to grow, however, reaching pretreatment volume after \sim 14 days (Figure 7C). A similar trend was observed for tumors cotreated with erlotinib and doxorubicin, although the initial reduction in tumor size was greater. In contrast, when mice were given erlotinib 8 hr prior to doxorubicin, the tumors not only exhibited a similar initial reduction in size, but also failed to regrow throughout the 14 day monitoring period. Thus, the chemosensitizing effect of sequential ERL \rightarrow DOX treatment seen in culture was also observed in vivo. These results suggest that time-staggered inhibition of EGFR, in combination with DNA damaging agents, could be a potentially useful therapeutic strategy for treating a subset of triple-negative tumors, particularly those with high basal levels of phosphorylated EGFR.



We next examined whether the principle of time-staggered inhibition would sensitize other breast cancer subtypes to doxorubicin. In contrast to BT-20 cells, MDA-MB-453 cells were not sensitized by sustained EGFR inhibition but instead were desensitized to DNA-damaging chemotherapy (Figure 1D). However, MDA-MB-453—and other widely used cell lines like BT-474—have a well-established oncogene addiction to HER2 (Neve et al., 2006). We therefore tested time-staggered inhibition of HER2 using the drug lapatinib (a potent inhibitor of both EGFR and HER2) in combination with doxorubicin in these cells. In both MDA-MB-453 and BT-474 cells, in contrast to the desensitization caused by pretreatment with erlotinib, we observed that lapatinib pretreatment enhanced sensitivity to doxorubicin to a similar extent as the enhancement observed with erlotinib in BT-20 and other EGFR-driven TNBC cells (Figures 7C and S7C). Importantly, whereas all temporal combinations of lapatinib and doxorubicin were synergistic in HER2-overexpressing cells, pretreatment with lapatinib resulted in the largest increase in apoptosis. Furthermore, caspase-8 cleavage was only observed following LAP → DOX treatment of HER2-driven cells, but not by other drug combinations. Knockdown of caspase-8 in these cells eliminated the specific component of enhanced cell death observed only in the pretreatment condition (Figures 7C and S7C), suggesting that this portion of the overall cell death was driven by caspase-8 activity.

Finally, we examined whether the efficacy of time-staggered inhibition of EGFR was limited to breast cancer cells. Many lung cancers, for example, contain either high levels of phosphorylated wild-type EGFR or mutations within EGFR itself. We therefore tested our ERL → DOX treatment protocol on NCI-H1650 cells, a lung cancer cell that contains an in-frame deletion that is commonly seen in lung cancers (Sordella et al., 2004), as well as on A549 and NCI-H358, cells that have high levels of phosphorylated wild-type EGFR, possibly due to HER2 amplification (Balko et al., 2006; Diaz et al., 2010; Helfrich et al., 2006; Rusnak et al., 2007). Remarkably, in all three lung cancer cell lines, we found that time-staggered inhibition of EGFR using erlotinib caused a dramatic sensitization to killing by doxorubicin that was associated with caspase-8 cleavage (Figures 7E, 7F, and S7D). Furthermore, knockdown of caspase-8 largely abrogated the enhanced cell death observed

in the pretreatment condition, exactly as was seen in the setting of TNBCs. Thus, time-staggered inhibition of EGFR in cells with highly active EGFR signaling may be a generalizable approach to potentiate the effects of DNA damaging chemotherapy.

DISCUSSION

In this study, we describe a systematic time- and dose-dependent approach to identifying drug combinations that are efficacious in killing cancer cells, depending on changes in the order and duration of drug exposure. We found that EGFR inhibition dramatically sensitizes a subset of TNBCs to DNA damage if the drugs are given sequentially, but not simultaneously. Furthermore, our transcriptional, proteomic, and computational analyses of signaling networks and phenotypes in drug-treated cells revealed that the enhanced treatment efficacy results from dynamic network rewiring of an oncogenic signature maintained by active EGFR signaling to unmask an apoptotic process that involves activation of caspase-8. The enhanced sensitivity to damaging agents that we observed required sustained inhibition of EGFR because the phenotype did not result from the rapid, direct inhibition of the oncogene but, rather, from modulation of an oncogene-driven transcriptional network as indicated schematically in the model shown in Figure 7G. Furthermore, our data suggest that it is activity of the EGFR pathway, rather than EGFR expression per se, that determines whether time-staggered inhibition will result in synergistic killing. Because EGFR can be activated through a diverse set of genetic alterations, some of which do not necessarily include EGFR itself (Sun et al., 2011), these findings highlight the need to understand network connectivity and dynamics (Pawson and Lindling, 2008). Conversely, these observations suggest that EGFR phosphorylation may constitute a useful biomarker of response to time-staggered inhibition in at least some tumor types that are EGFR driven, including some TNBCs and lung cancers.

A key consequence of the erlotinib-dependent dynamic remodeling of the DDR network is activation of caspase-8 following DNA damage. The mechanism of caspase-8 activation is unclear because it is generally thought to be specific to receptor-mediated apoptosis triggered by ligands such as the tumor necrosis factor (TNF) and TNF-related apoptosis-inducing

Figure 7. Time-Staggered Inhibition of EGFR Signaling Enhances Apoptotic Response in a Subset of TNBC Cells and Other EGFR-Driven Cells

(A) Panel of TNBC cell lines with a wide range of EGFR expression levels. Heatmap for total EGFR expression, p-EGFR (Y1173), percent apoptosis, apoptosis relative to DOX alone, and casp-8 cleavage. Apoptosis measured as in Figure 1. EGFR and p-EGFR expression are measured by western blotting of untreated cells. Cleaved casp-8 measured by western blot 8 hr after exposure to DOX.

(B) EGFR activity, but not total EGFR expression, is correlated with sensitivity to time-staggered ERL → DOX combination. Fold enrichment of cell death observed in E → D relative to DOX alone regressed against total EGFR or p-EGFR (pY1173) as measured in untreated cells for the ten TNBC cell lines shown in Figure 7A. R^2 reports the linear fit for each trend line.

(C) BT-20 cells grown as xenograft tumors in nude mice. Arrow indicates intraperitoneal administration of indicated drugs. Mean tumor volume \pm SEM shown from four animals for each treatment condition.

(D–F) Time-staggered inhibition of HER2 in HER2-driven breast cancer cells (D) or EGFR in lung cancer cells (E and F) causes casp-8 activation and sensitization to DOX. Apoptosis measured as in Figure 1 for cells exposed to a control RNA (left in each panel) or siRNA targeting casp-8 (right in each panel). Caspase-8 activation was monitored 8 hr after doxorubicin treatment (c-casp8, shown beneath the control RNA plots). Validation of caspase-8 knockdown is shown below the CASP8 siRNA plots. Mean values \pm SD of three experiments are shown. (D) HER2-overexpressing MDA-MB-453 cells treated with lapatinib. (E and F) Lung cancer cells treated with erlotinib. (E) NCI-H1650. (F) A-549.

(G) A model for enhanced cell death after DNA damage by chronic EGFR inhibition in triple-negative breast cancer cells.

See also Figure S7.

ligand (TRAIL). Possibilities include feedback activation by caspase-3, possibly involving caspase-6 (Albeck et al., 2008); direct activation of death receptors by DDR proteins (Yoon et al., 2009); or an autocrine/paracrine mechanism involving an as-yet unidentified death ligand. Distinguishing between these and other possibilities will be a focus for future studies.

Combinatorial drug effects are complex, even for relatively specific drugs like EGFR inhibitors. Our understanding of compensation and network rewiring is currently not sufficient to allow a priori predictions of the cellular response, particularly in cancer cells in which signaling networks often exist in atypical forms. Our work highlights the utility of experimental examination of time-staggered combination treatments for their anticancer effects, particularly when combined with an analysis of signaling pathways and responses using mathematical modeling. These types of approaches may facilitate the identification of efficacious drug combinations and new therapeutic targets and also the design of different types of clinical trials to study the killing of oncogene-addicted tumors through drug-induced dynamic rewiring of signaling pathways.

EXPERIMENTAL PROCEDURES

Cellular Response Assays

Apoptosis

Following the treatment time course, cells were washed, trypsinized, fixed in 4% paraformaldehyde for 15 min at room temperature, resuspended in ice-cold methanol, and incubated overnight at -20°C . Cells were then washed twice in PBS-Tween and stained with antibodies against cleaved caspase-3 and poly(ADP-ribose) polymerase (PARP). Secondary Alexa-conjugated antibodies were used for visualization in a BD FACS Caliber flow cytometer.

Cell-Cycle Analysis

Cells were fixed in 70% ethanol overnight at -20°C , permeabilized with 0.25% Triton X-100 for 20 min at 4°C , blocked with 1% BSA, and incubated with anti-phospho-histone H3. Following washing, cells were incubated with Alexa488-conjugated secondary antibody on ice, washed, and stained with propidium iodide (PI) prior to analysis. Data were analyzed using the Dean-Jett-Fox algorithm.

Cell Viability/Proliferation

Cells were plated at 5,000 cells per well in 96-well plates. Metabolic viability was determined using CellTiterGlo (Promega) according to the manufacturer's protocol.

Western Blotting and Antibodies

Cells were lysed in a manner that would allow samples to be used for both western blot analysis and reverse-phase protein microarray. See [Extended Experimental Procedures](#) for a detailed description of the cell lysis protocol and antibodies used in this study.

Data generated by quantitative western blot were preprocessed prior to use in computational modeling. Raw signals for each protein target of interest were quantified and background subtracted using the Li-COR Odyssey software and divided by β -actin signals to normalize for loading differences, and then each normalized signal was divided by a reference sample contained on each gel for gel-to-gel normalization.

Reverse-Phase Protein Microarray

Reverse-phase protein microarrays were printed on a fee-for-service basis through Aushon Biosystems. Validation of antibodies, staining, and analysis of array data was performed as described previously (Sevecka and MacBeath, 2006).

Immunofluorescence Microscopy

Cells were seeded onto coverslips and treated for the indicated times. For autophagy analysis, cells were stably transfected with an mCHERRY-GFP-LC3

reporter construct. Cells were fixed and stained with primary antibody targeting either p-H2AX or 53BP1 and DAPI as above. Data reported are integrated intensity of p-H2AX or 53BP1 foci per nucleus. For autophagy measurements, cells were scored positive if the number of GFP and mCHERRY puncta significantly increased relative to untreated cells. Approximately 100 cells were counted in a double-blind fashion per condition. Each experiment was performed in experimental triplicate.

RNA Expression Analysis by Microarray

RNA was extracted from cells using the RNeasy Kit (QIAGEN). Affymetrix Human U133 Plus 2.0 microarrays were hybridized, labeled, and processed on a fee-for-service basis through the MIT BioMicro Center. Microarray data were obtained from three independent biological replicates per time point and analyzed using *linear model for microarray* (LIMMA).

Computational Modeling and Statistics

Unless otherwise noted, all statistical analyses were performed using Graphpad Prism, and graphs were created using Microsoft Excel, Spotfire, Matlab, DataRail, or SIMCA-P. Analysis of flow cytometry data was performed using FloJo. Analysis of RNA expression microarray data was performed using either GSEA or GeneGO as indicated.

Data-Driven Modeling

Data-driven modeling and the application of partial least-squares to biological data have been described in detail previously (Janes and Yaffe, 2006). All data were variance scaled to nondimensionalize the different measurements. Model predictions were made via cross-validation. Model fitness was calculated using R^2 , Q^2 , and RMSE, as described previously by Gaudet et al. (2005). VIP was calculated following Janes et al. (2008).

Xenograft Tumor Model

For in vivo tumor regression assays, 10^7 BT-20 cells in PBS were mixed 1:1 with matrigel on ice and injected subcutaneously into the hindflanks of nude mice (NCR nu/nu, Taconic). Tumors were allowed to form for 7 days. Mice were then treated intraperitoneally with doxorubicin (4 mg/kg) or a combination of doxorubicin and erlotinib (25 mg/kg), with erlotinib either given at the same time as doxorubicin (D/E) or given 8 hr prior to doxorubicin (E \rightarrow D). Tumors were monitored for 14 days after the treatment phase, and volume was estimated using the $\frac{1}{2} L \times W^2$ formula. These experiments were approved by the Massachusetts Institute of Technology Committee on Animal Care (CAC).

ACCESSION NUMBERS

Expression data can be found in the GEO repository under the accession number GSE30516.

SUPPLEMENTAL INFORMATION

Supplemental information includes Extended Experimental Procedures, seven figures, and one table and can be found with this article online at [doi:10.1016/j.cell.2012.03.031](https://doi.org/10.1016/j.cell.2012.03.031).

ACKNOWLEDGMENTS

We thank Sandra Morandell, Kylie Huang, Jose McFaline, and Jessica Reddy for technical assistance in the early stages of this study and the Swanson Biotechnology Center at the Koch Institute for their technical support, including Eliza Vasile (microscopy), Glen Paradis (flow cytometry), and especially Charlie Whittaker (bioinformatics) for his guidance in analyzing microarray experiments. We further thank Doug Lauffenburger and members of the CDP community for fruitful discussions and advice throughout the development and execution of this study. This work was supported by NIH grants CA112967 and GM68762 to P.K.S. and M.B.Y., ES015339 to M.B.Y., and DOD fellowship BC097884 to M.J.L. P.K.S., G.M., and M.B.Y. are founders and shareholders of Merrimack Pharmaceuticals. P.K.S. and M.B.Y. are scientific advisory board members, and G.M. is a current employee. G.M. is also a scientific advisory board member of Aushon Biosystems.

Received: September 9, 2011

Revised: December 6, 2011

Accepted: March 2, 2012

Published: May 10, 2012

REFERENCES

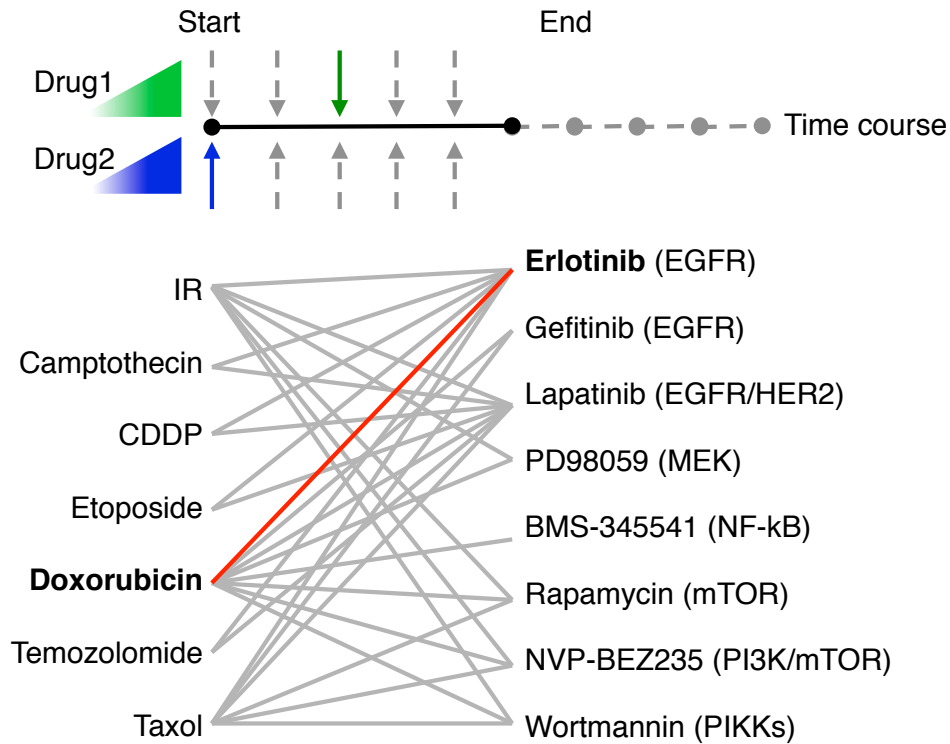
- Abeloff, M., Wolff, A., Weber, B., Zaks, T., Sacchini, V., and McCormick, B. (2008). Cancer of the breast. In *Abeloff's Clinical Oncology*, M. Abeloff, J. Armitage, J. Niederhuber, M. Kastan, and W. McKenna, eds. (Maryland Heights, MO: Churchill Livingstone), pp. 1875–1944.
- Albeck, J.G., Burke, J.M., Spencer, S.L., Lauffenburger, D.A., and Sorger, P.K. (2008). Modeling a snap-action, variable-delay switch controlling extrinsic cell death. *PLoS Biol.* 6, 2831–2852.
- Balko, J.M., Potti, A., Saunders, C., Stromberg, A., Haura, E.B., and Black, E.P. (2006). Gene expression patterns that predict sensitivity to epidermal growth factor receptor tyrosine kinase inhibitors in lung cancer cell lines and human lung tumors. *BMC Genomics* 7, 289.
- Bosch, A., Eroles, P., Zaragoza, R., Viña, J.R., and Lluch, A. (2010). Triple-negative breast cancer: molecular features, pathogenesis, treatment and current lines of research. *Cancer Treat. Rev.* 36, 206–215.
- Carey, L., Rugo, H., Marcom, P., Irvin, W., Ferraro, M., Burrows, E., He, X., Perou, C., and Winer, E. (2008). TBCRC 001: EGFR inhibition with cetuximab added to carboplatin in metastatic triple-negative (basal-like) breast cancer. *J. Clin. Oncol.* 26, 26–31.
- Chou, T.C., and Talalay, P. (1984). Quantitative analysis of dose-effect relationships: the combined effects of multiple drugs or enzyme inhibitors. *Adv. Enzyme Regul.* 22, 27–55.
- Corkery, B., Crown, J., Clynes, M., and O'Donovan, N. (2009). Epidermal growth factor receptor as a potential therapeutic target in triple-negative breast cancer. *Ann. Oncol.* 20, 862–867.
- Dent, R., Trudeau, M., Pritchard, K.I., Hanna, W.M., Kahn, H.K., Sawka, C.A., Lickley, L.A., Rawlinson, E., Sun, P., and Narod, S.A. (2007). Triple-negative breast cancer: clinical features and patterns of recurrence. *Clin. Cancer Res.* 13, 4429–4434.
- Diaz, R., Nguema, P.A., Parrondo, R., Perez-Stable, C., Manrique, I., Redrado, M., Catena, R., Collantes, M., Peñuelas, I., Díaz-González, J.A., and Calvo, A. (2010). Antitumor and antiangiogenic effect of the dual EGFR and HER-2 tyrosine kinase inhibitor lapatinib in a lung cancer model. *BMC Cancer* 10, 188.
- Ekins, S., Nikolsky, Y., Bugrim, A., Kirillov, E., and Nikolskaya, T. (2007). Pathway mapping tools for analysis of high content data. *Methods Mol. Biol.* 356, 319–350.
- Fitzgerald, J.B., Schoeberl, B., Nielsen, U.B., and Sorger, P.K. (2006). Systems biology and combination therapy in the quest for clinical efficacy. *Nat. Chem. Biol.* 2, 458–466.
- Gaudet, S., Janes, K.A., Albeck, J.G., Pace, E.A., Lauffenburger, D.A., and Sorger, P.K. (2005). A compendium of signals and responses triggered by pro-death and prosurvival cytokines. *Mol. Cell. Proteomics* 4, 1569–1590.
- Hanahan, D., and Weinberg, R.A. (2000). The hallmarks of cancer. *Cell* 100, 57–70.
- Harper, J.W., and Elledge, S.J. (2007). The DNA damage response: ten years after. *Mol. Cell* 28, 739–745.
- Helfrich, B.A., Raben, D., Varella-Garcia, M., Gustafson, D., Chan, D.C., Bemis, L., Coldren, C., Barón, A., Zeng, C., Franklin, W.A., et al. (2006). Antitumor activity of the epidermal growth factor receptor (EGFR) tyrosine kinase inhibitor gefitinib (ZD1839, Iressa) in non-small cell lung cancer cell lines correlates with gene copy number and EGFR mutations but not EGFR protein levels. *Clin. Cancer Res.* 12, 7117–7125.
- Janes, K.A., Albeck, J.G., Gaudet, S., Sorger, P.K., Lauffenburger, D.A., and Yaffe, M.B. (2005). A systems model of signaling identifies a molecular basis set for cytokine-induced apoptosis. *Science* 310, 1646–1653.
- Janes, K.A., Reinhardt, H.C., and Yaffe, M.B. (2008). Cytokine-induced signaling networks prioritize dynamic range over signal strength. *Cell* 135, 343–354.
- Janes, K.A., and Yaffe, M.B. (2006). Data-driven modelling of signal-transduction networks. *Nat. Rev. Mol. Cell Biol.* 7, 820–828.
- Kang, N., Zhang, J.H., Qiu, F., Tashiro, S., Onodera, S., and Ikejima, T. (2010). Inhibition of EGFR signaling augments oridonin-induced apoptosis in human laryngeal cancer cells via enhancing oxidative stress coincident with activation of both the intrinsic and extrinsic apoptotic pathways. *Cancer Lett.* 294, 147–158.
- Kim, R. (2005). Recent advances in understanding the cell death pathways activated by anticancer therapy. *Cancer* 103, 1551–1560.
- Lichter, A.S., and Lawrence, T.S. (1995). Recent advances in radiation oncology. *N. Engl. J. Med.* 332, 371–379.
- Lopez, J.P., Wang-Rodriguez, J., Chang, C., Chen, J.S., Pardo, F.S., Aguilera, J., and Ongkeko, W.M. (2007). Gefitinib inhibition of drug resistance to doxorubicin by inactivating ABCG2 in thyroid cancer cell lines. *Arch. Otolaryngol. Head Neck Surg.* 133, 1022–1027.
- MacBeath, G. (2002). Protein microarrays and proteomics. *Nat. Genet. Suppl.* 32, 526–532.
- Montesano, R., Drevon, C., Kuroki, T., Saint Vincent, L., Handleman, S., Sanford, K.K., DeFeo, D., and Weinstein, I.B. (1977). Test for malignant transformation of rat liver cells in culture: cytology, growth in soft agar, and production of plasminogen activator. *J. Natl. Cancer Inst.* 59, 1651–1658.
- Morgillo, F., D'Aiuto, E., Troiani, T., Martinelli, E., Cascone, T., De Palma, R., Orditura, M., De Vita, F., and Ciardiello, F. (2011). Antitumor activity of bortezomib in human cancer cells with acquired resistance to anti-epidermal growth factor receptor tyrosine kinase inhibitors. *Lung Cancer* 71, 283–290.
- Neve, R.M., Chin, K., Fridlyand, J., Yeh, J., Baehner, F.L., Fevr, T., Clark, L., Bayani, N., Coppe, J.P., Tong, F., et al. (2006). A collection of breast cancer cell lines for the study of functionally distinct cancer subtypes. *Cancer Cell* 10, 515–527.
- Pawson, T., and Linding, R. (2008). Network medicine. *FEBS Lett.* 582, 1266–1270.
- Perou, C.M., Sørlie, T., Eisen, M.B., van de Rijn, M., Jeffrey, S.S., Rees, C.A., Pollack, J.R., Ross, D.T., Johnsen, H., Akslen, L.A., et al. (2000). Molecular portraits of human breast tumours. *Nature* 406, 747–752.
- Rusnak, D.W., Alligood, K.J., Mullin, R.J., Spehar, G.M., Arenas-Elliott, C., Martin, A.M., Degenhardt, Y., Rudolph, S.K., Haws, T.F., Jr., Hudson-Curtis, B.L., and Gilmer, T.M. (2007). Assessment of epidermal growth factor receptor (EGFR, ErbB1) and HER2 (ErbB2) protein expression levels and response to lapatinib (Tykerb, GW572016) in an expanded panel of human normal and tumour cell lines. *Cell Prolif.* 40, 580–594.
- Sachs, K., Perez, O., Pe'er, D., Lauffenburger, D.A., and Nolan, G.P. (2005). Causal protein-signaling networks derived from multiparameter single-cell data. *Science* 308, 523–529.
- Schechter, A.L., Stern, D.F., Vaidyanathan, L., Decker, S.J., Drebin, J.A., Greene, M.I., and Weinberg, R.A. (1984). The neu oncogene: an erb-B-related gene encoding a 185,000-Mr tumour antigen. *Nature* 312, 513–516.
- Sevecka, M., and MacBeath, G. (2006). State-based discovery: a multidimensional screen for small-molecule modulators of EGF signaling. *Nat. Methods* 3, 825–831.
- Slamon, D.J., Clark, G.M., Wong, S.G., Levin, W.J., Ullrich, A., and McGuire, W.L. (1987). Human breast cancer: correlation of relapse and survival with amplification of the HER-2/neu oncogene. *Science* 235, 177–182.
- Sordella, R., Bell, D.W., Haber, D.A., and Settleman, J. (2004). Gefitinib-sensitizing EGFR mutations in lung cancer activate anti-apoptotic pathways. *Science* 305, 1163–1167.
- Sørlie, T., Perou, C.M., Tibshirani, R., Aas, T., Geisler, S., Johnsen, H., Hastie, T., Eisen, M.B., van de Rijn, M., Jeffrey, S.S., et al. (2001). Gene expression patterns of breast carcinomas distinguish tumor subclasses with clinical implications. *Proc. Natl. Acad. Sci. USA* 98, 10869–10874.
- Subramanian, A., Tamayo, P., Mootha, V.K., Mukherjee, S., Ebert, B.L., Gillette, M.A., Paulovich, A., Pomeroy, S.L., Golub, T.R., Lander, E.S., and Mesirov, J.P. (2005). Gene set enrichment analysis: a knowledge-based

- approach for interpreting genome-wide expression profiles. *Proc. Natl. Acad. Sci. USA* **102**, 15545–15550.
- Sun, T., Aceto, N., Meerbrey, K.L., Kessler, J.D., Zhou, C., Migliaccio, I., Nguyen, D.X., Pavlova, N.N., Botero, M., Huang, J., et al. (2011). Activation of multiple proto-oncogenic tyrosine kinases in breast cancer via loss of the PTPN12 phosphatase. *Cell* **144**, 703–718.
- Turner, J.G., Gump, J.L., Zhang, C., Cook, J.M., Marchion, D., Hazlehurst, L., Munster, P., Schell, M.J., Dalton, W.S., and Sullivan, D.M. (2006). ABCG2 expression, function, and promoter methylation in human multiple myeloma. *Blood* **108**, 3881–3889.
- Winer, E.P., and Mayer, E.L. (2007). Optimizing treatment of “triple-negative” breast cancer. *SABCS 2007: Improving Outcomes in Advanced and Metastatic Breast Cancer*. <http://www.medscape.org/viewarticle/569483>.
- Woehlecke, H., Osada, H., Herrmann, A., and Lage, H. (2003). Reversal of breast cancer resistance protein-mediated drug resistance by tryprostatin A. *Int. J. Cancer* **107**, 721–728.
- Wood, E.R., Truesdale, A.T., McDonald, O.B., Yuan, D., Hassell, A., Dickerson, S.H., Ellis, B., Pennisi, C., Horne, E., Lackey, K., et al. (2004). A unique structure for epidermal growth factor receptor bound to GW572016 (Lapatinib): relationships among protein conformation, inhibitor off-rate, and receptor activity in tumor cells. *Cancer Res.* **64**, 6652–6659.
- Yoon, C.H., Kim, M.J., Park, M.T., Byun, J.Y., Choi, Y.H., Yoo, H.S., Lee, Y.M., Hyun, J.W., and Lee, S.J. (2009). Activation of p38 mitogen-activated protein kinase is required for death receptor-independent caspase-8 activation and cell death in response to sphingosine. *Mol. Cancer Res.* **7**, 361–370.

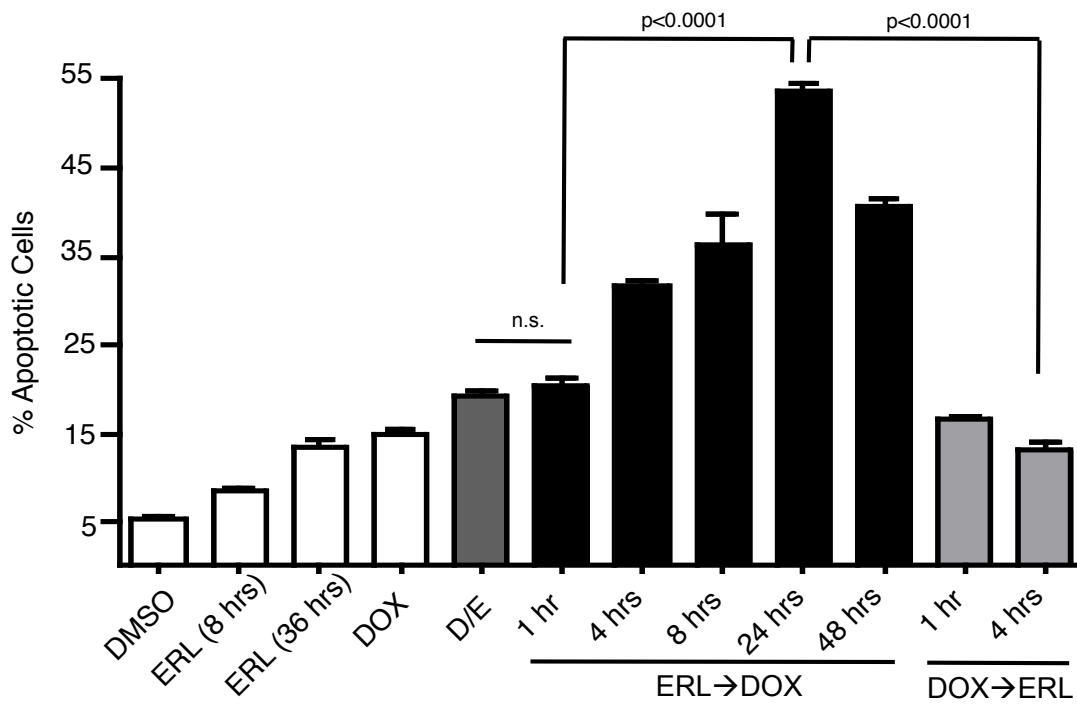
SUPPORTING DATA

Lee, MJ Figure 1

A

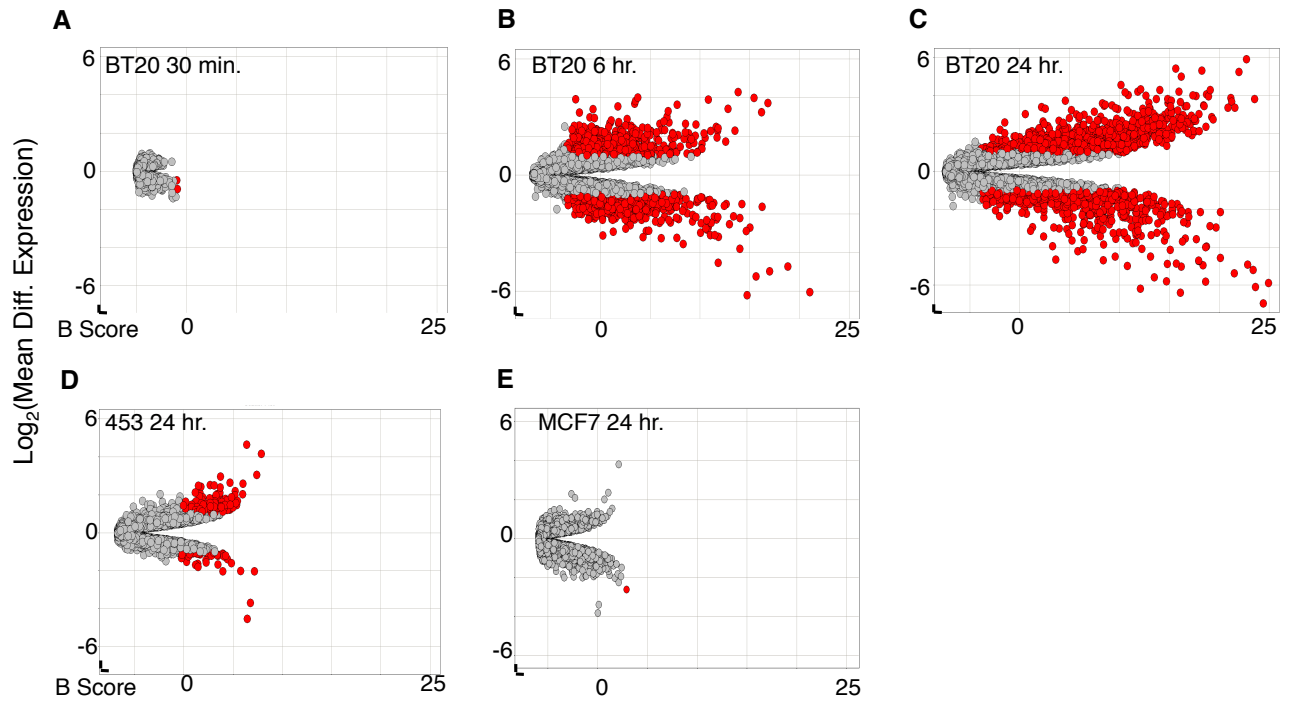


B



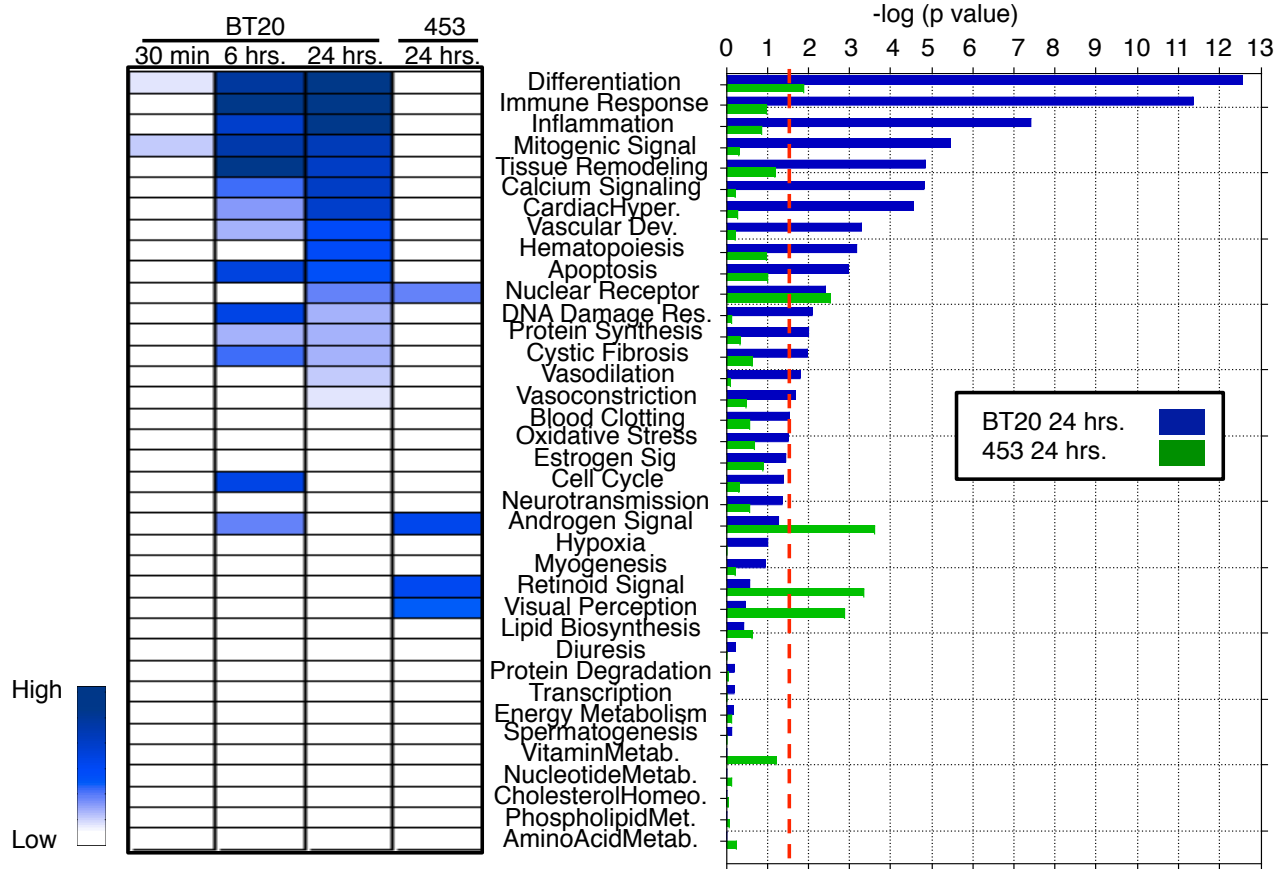
SUPPORTING DATA

Lee, MJ Figure 2



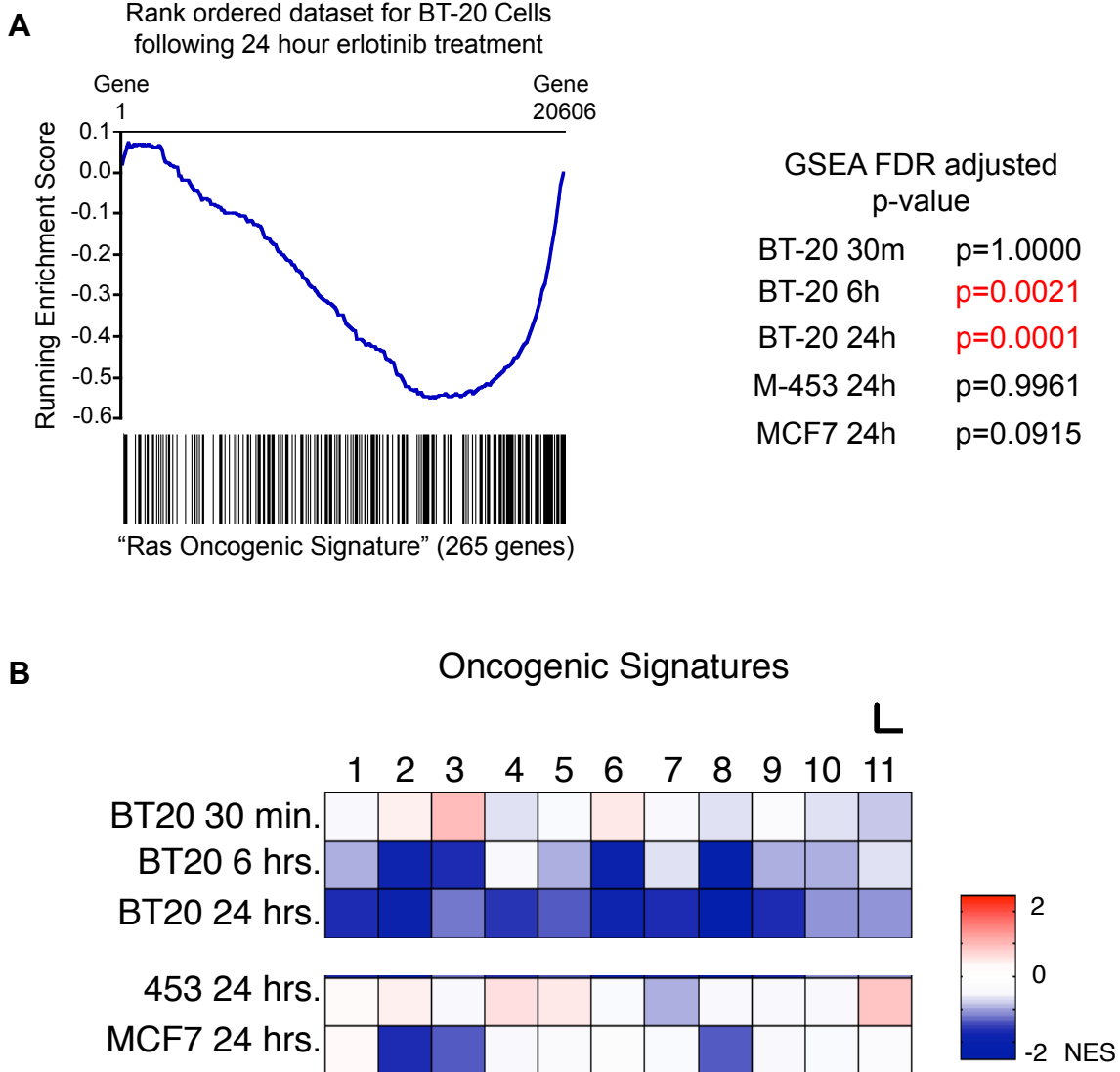
SUPPORTING DATA

Lee, MJ Figure 3



SUPPORTING DATA

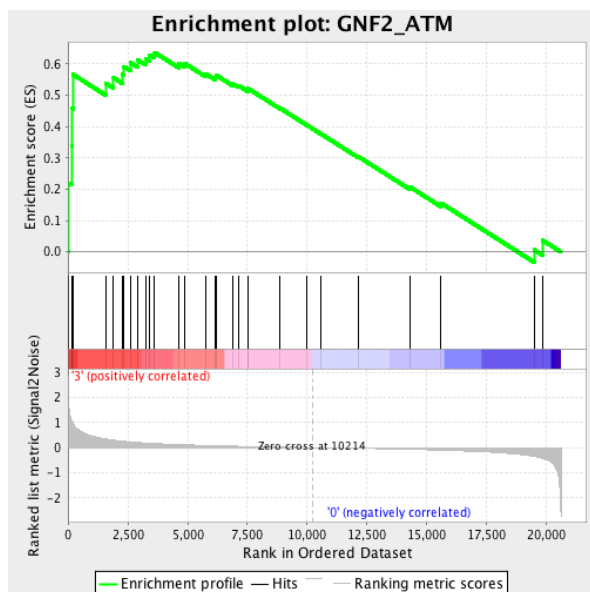
Lee, MJ Figure 4



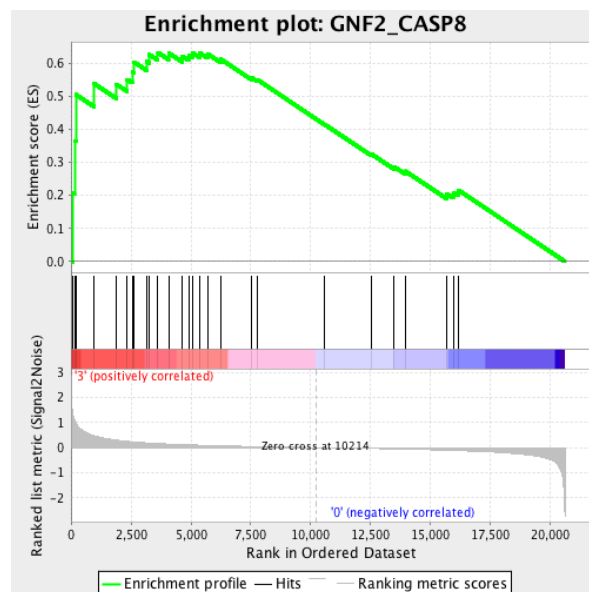
SUPPORTING DATA

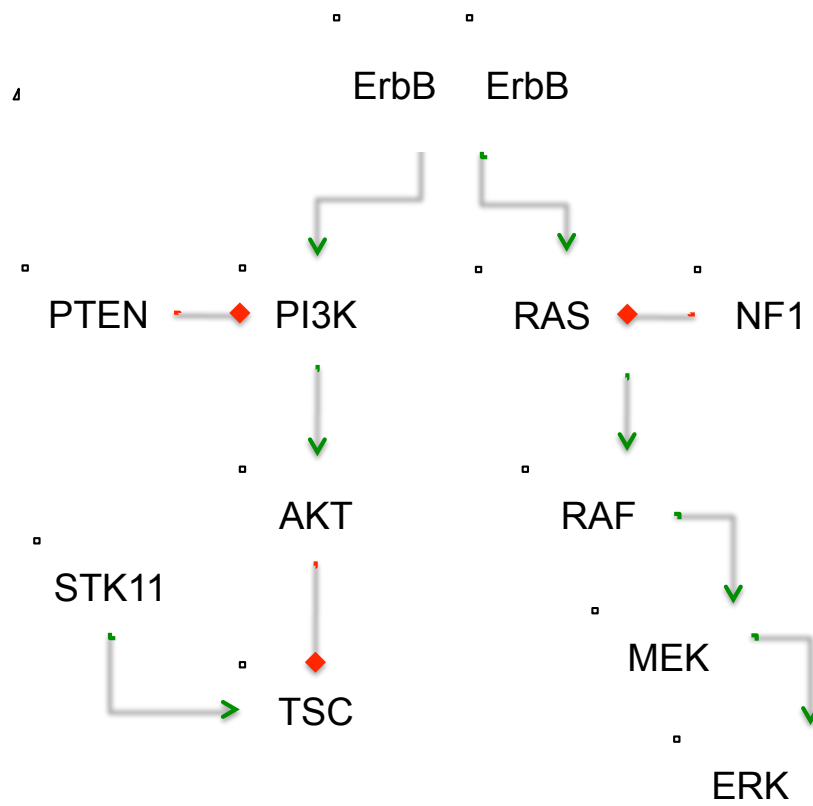
Lee, MJ Figure 5

A

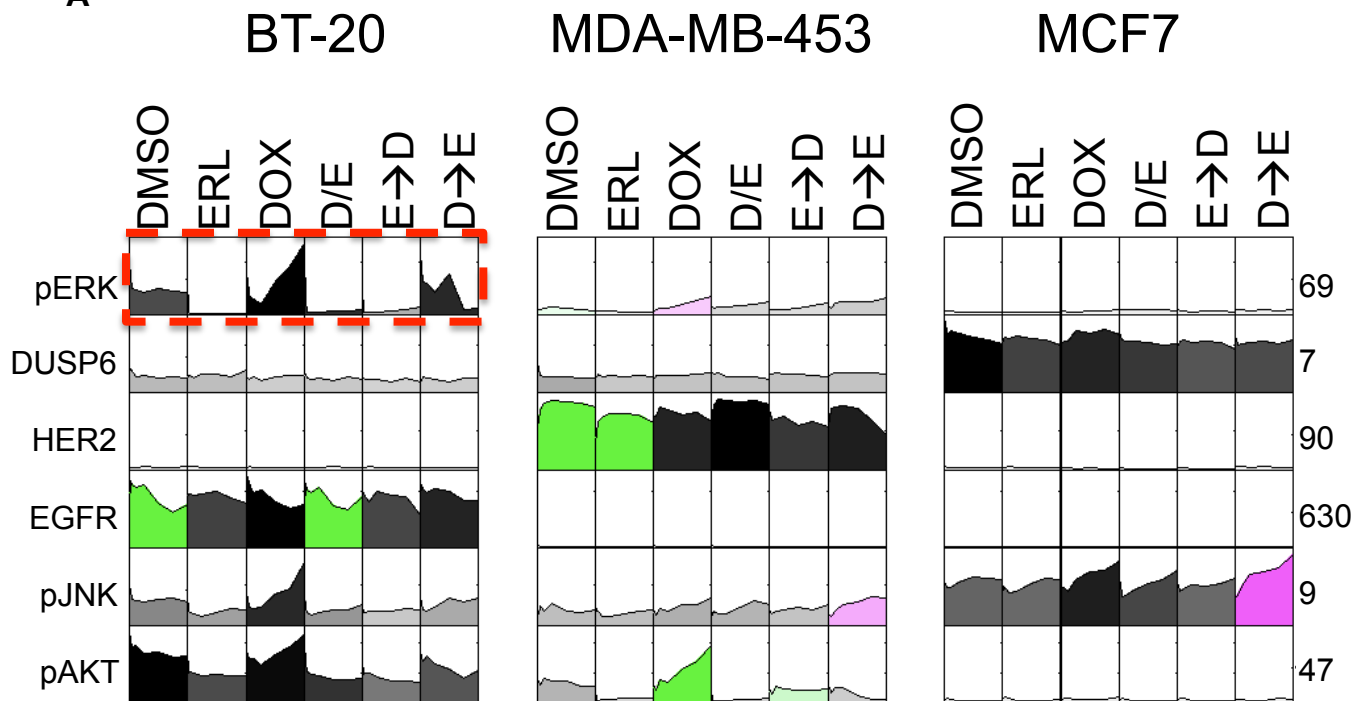


B



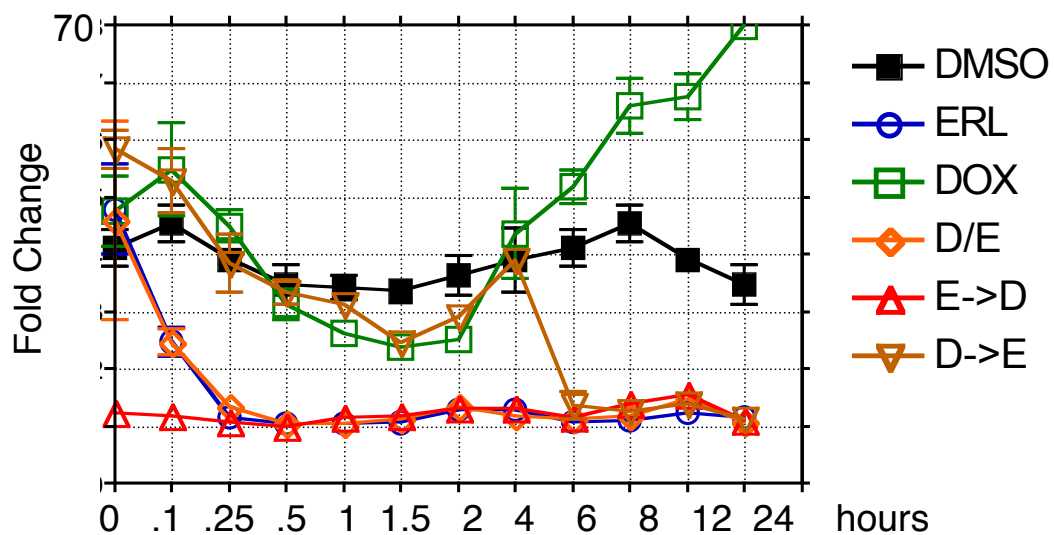


A

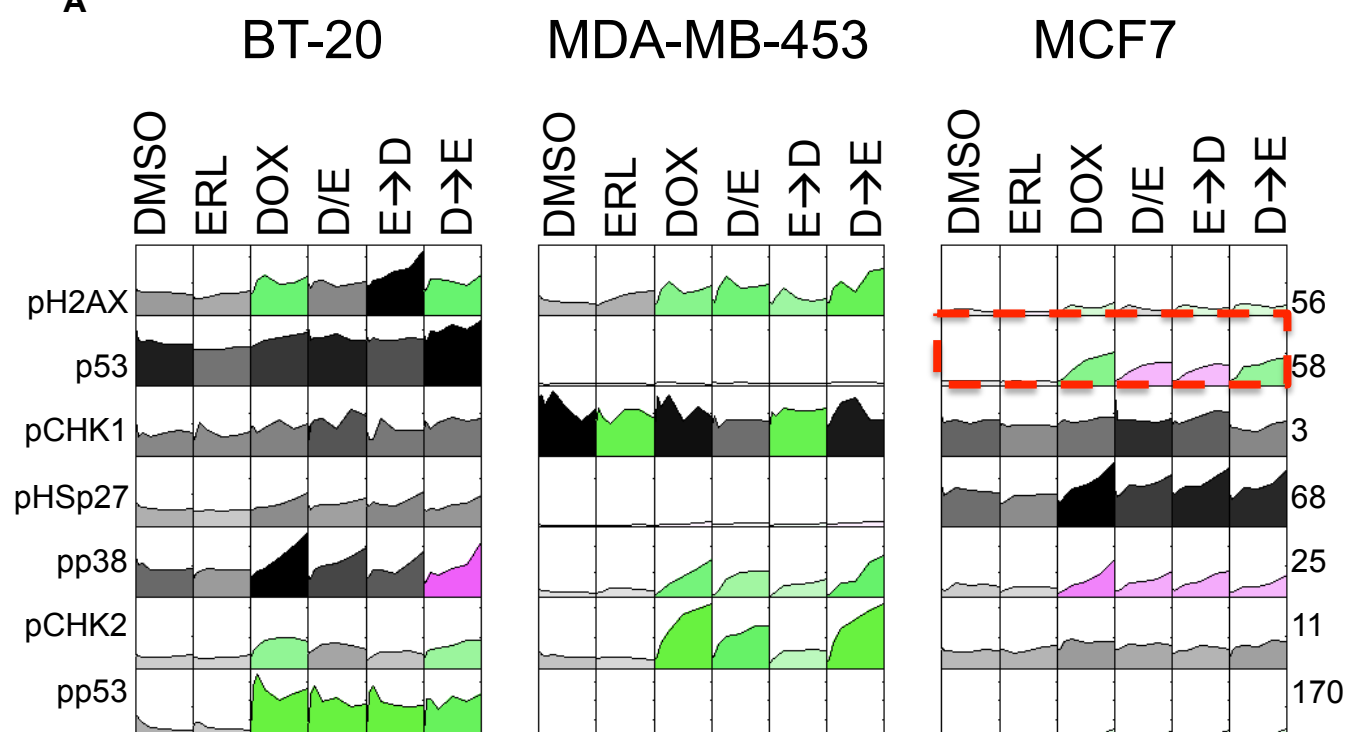


B

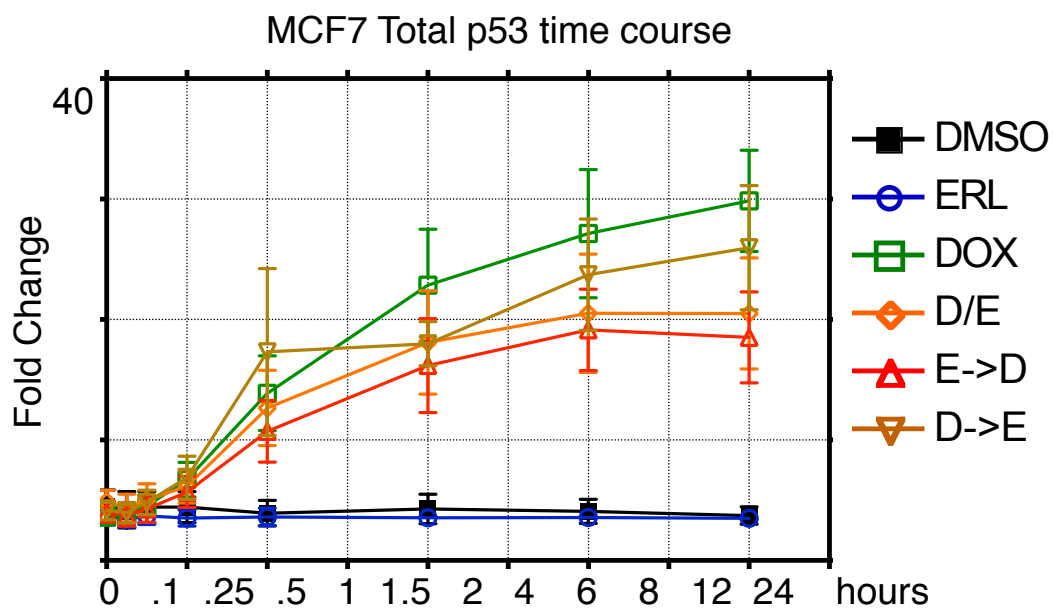
BT20 p-ERK time course



A

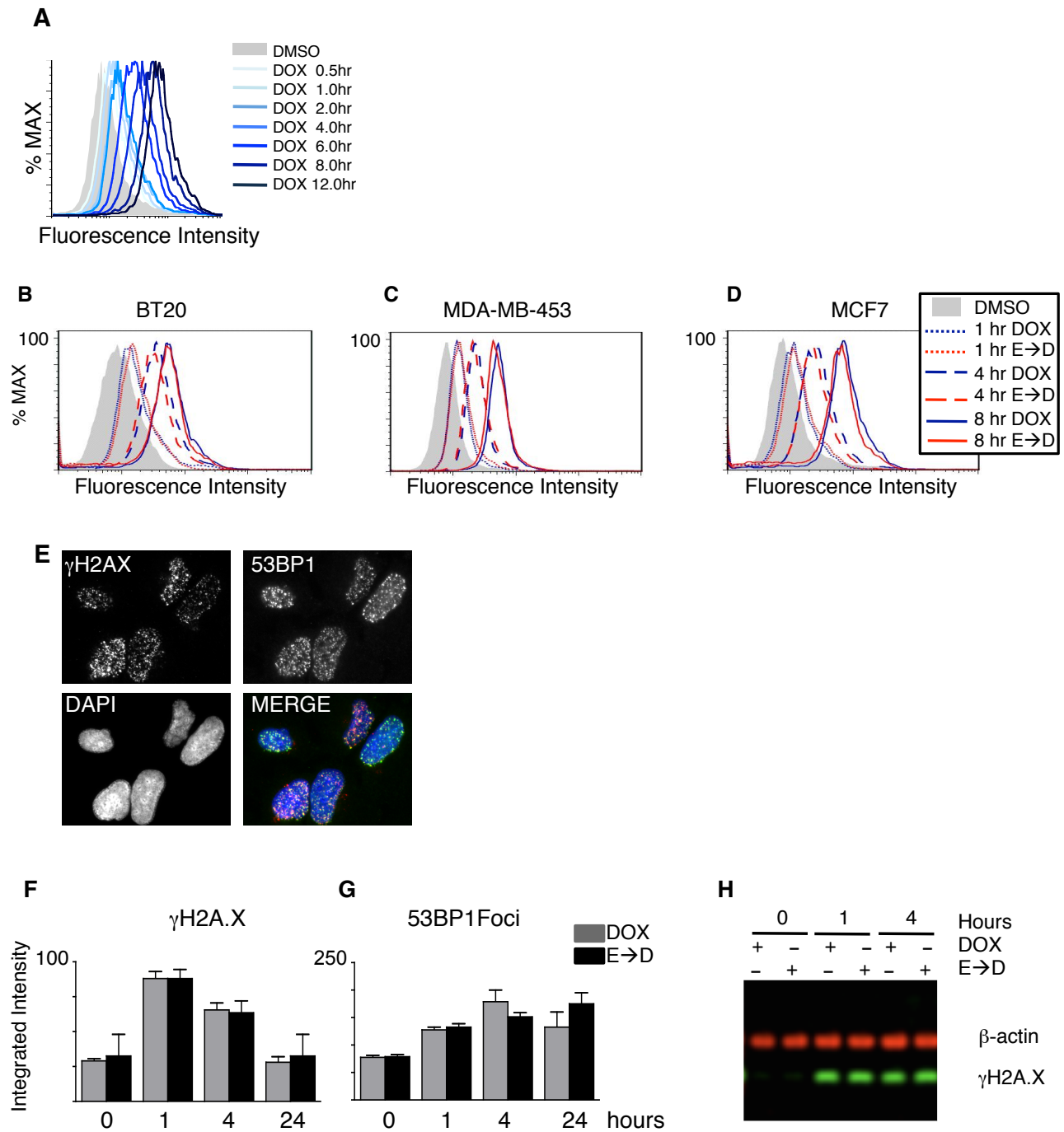


B



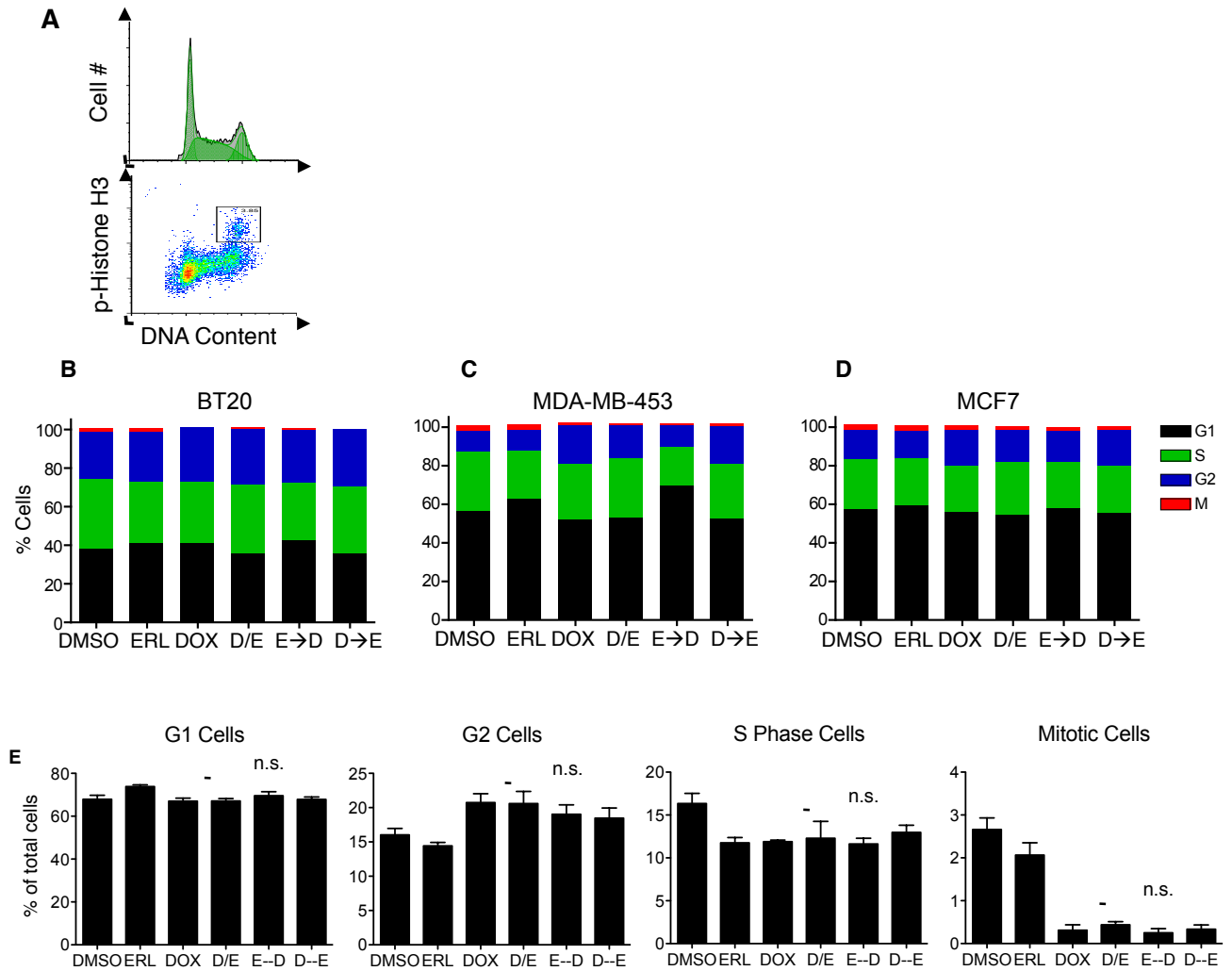
SUPPORTING DATA

Lee, MJ Figure 9

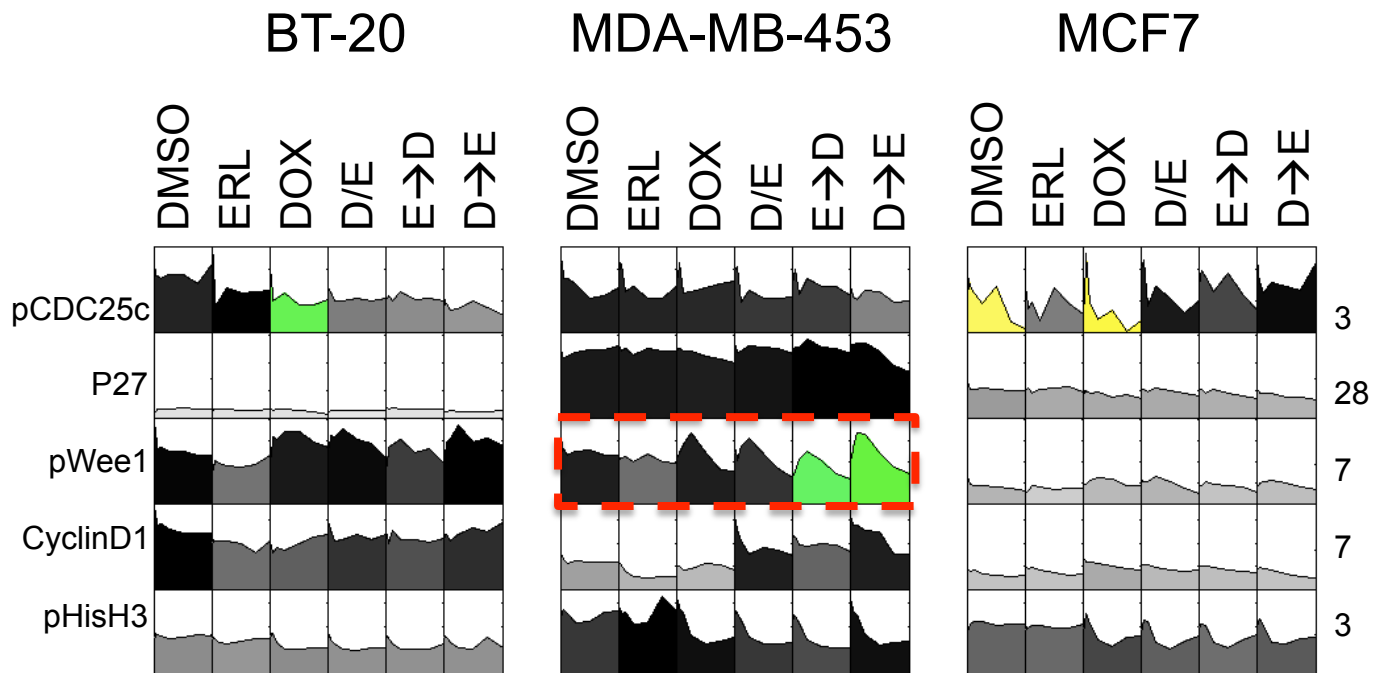


SUPPORTING DATA

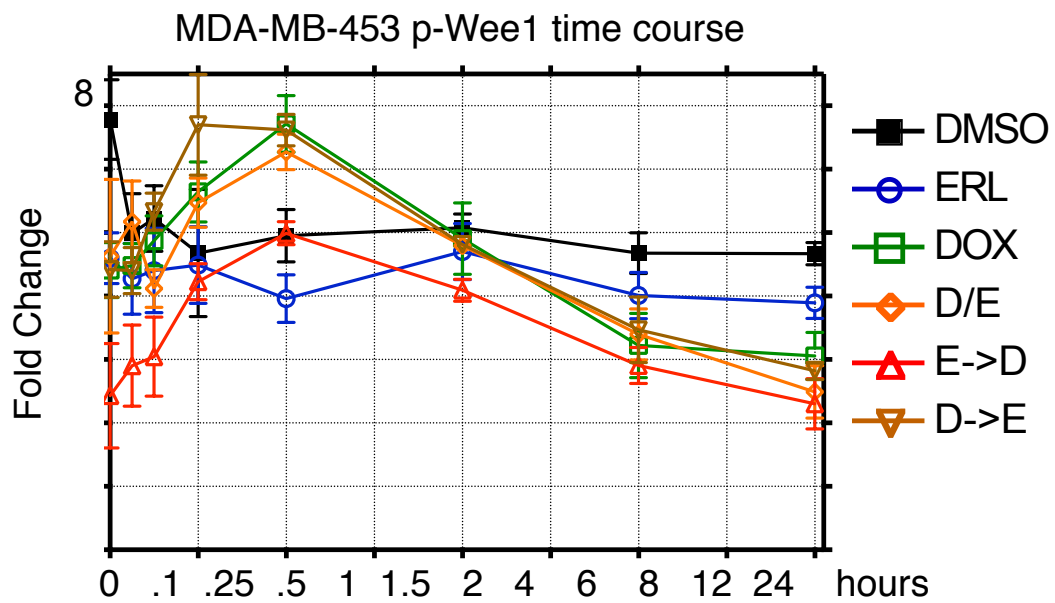
Lee, MJ Figure 10

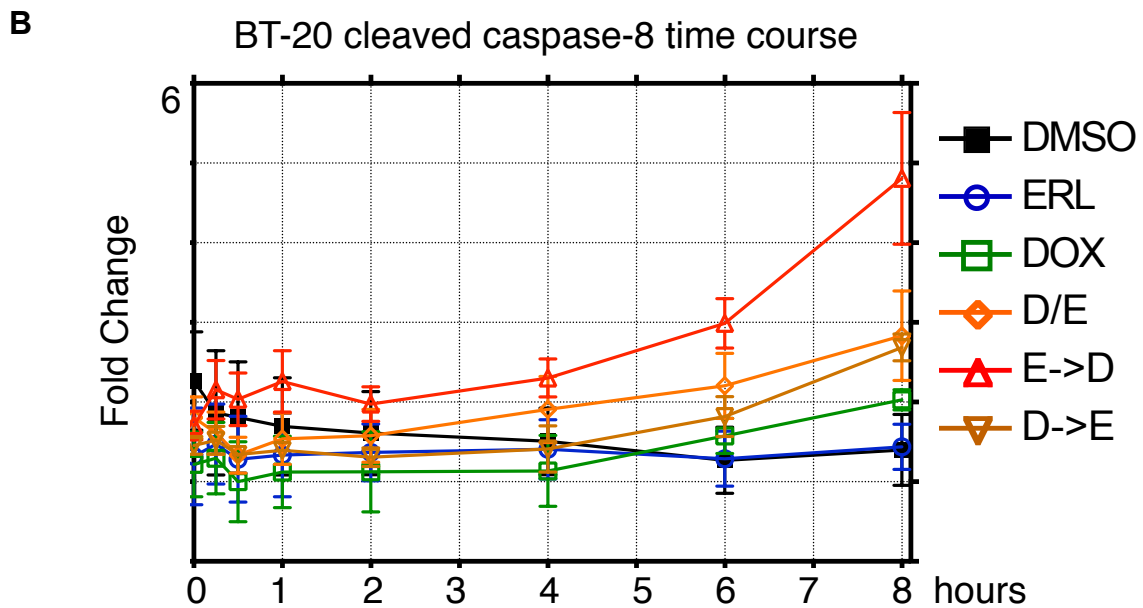
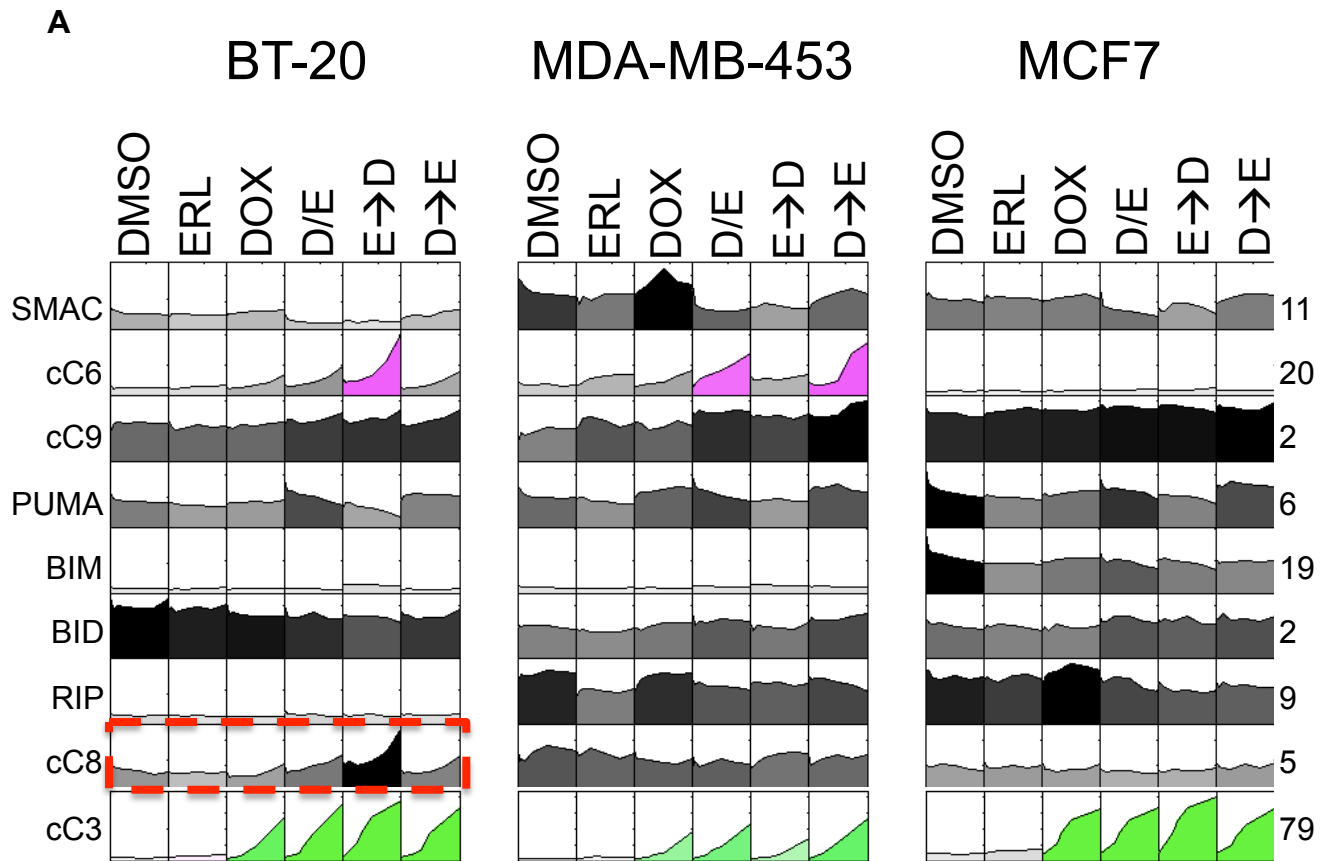


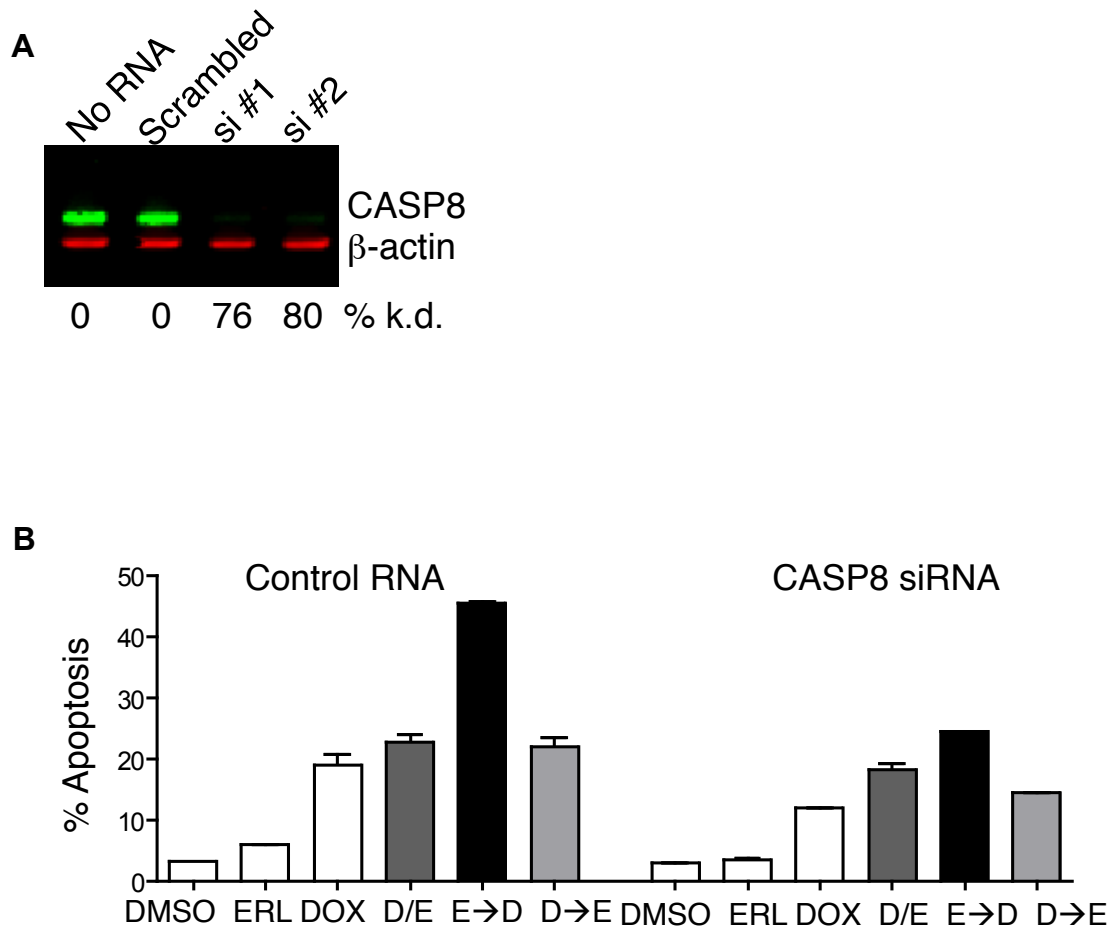
A



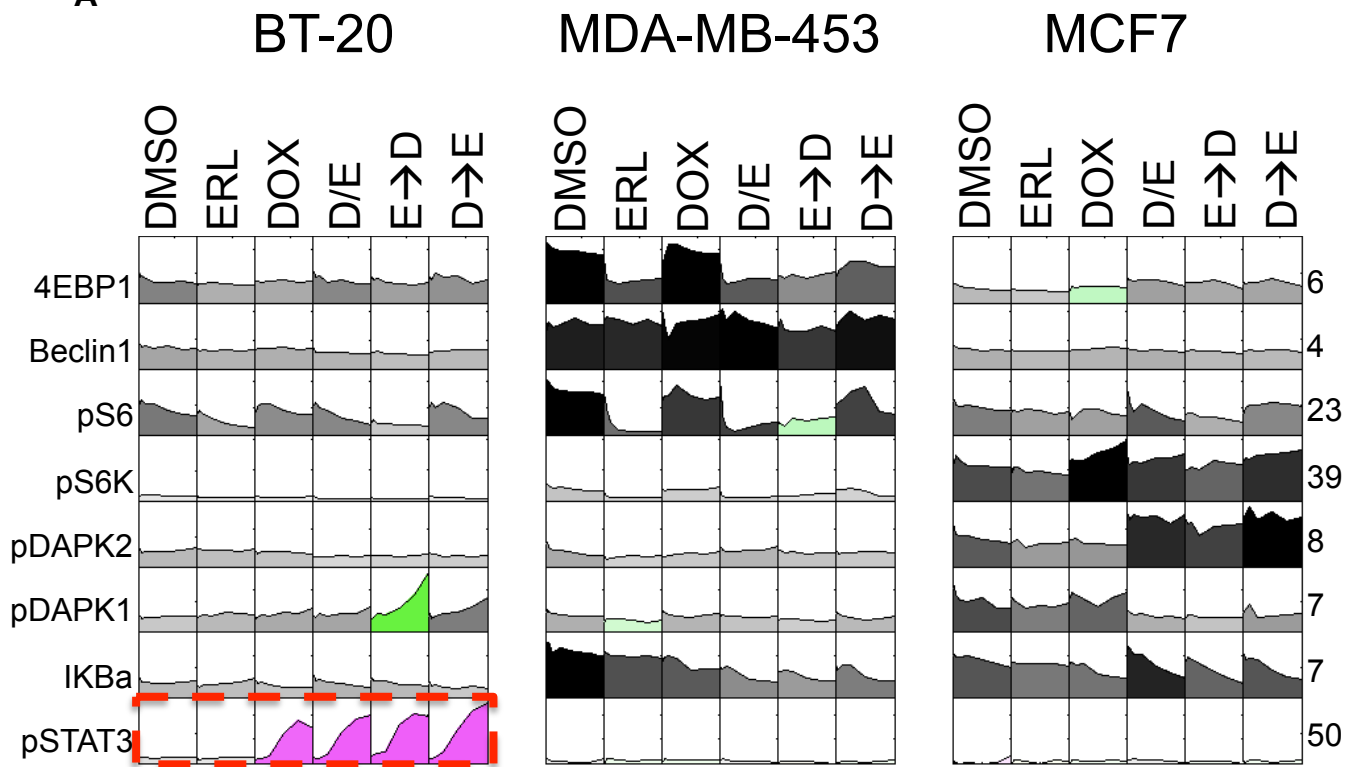
B



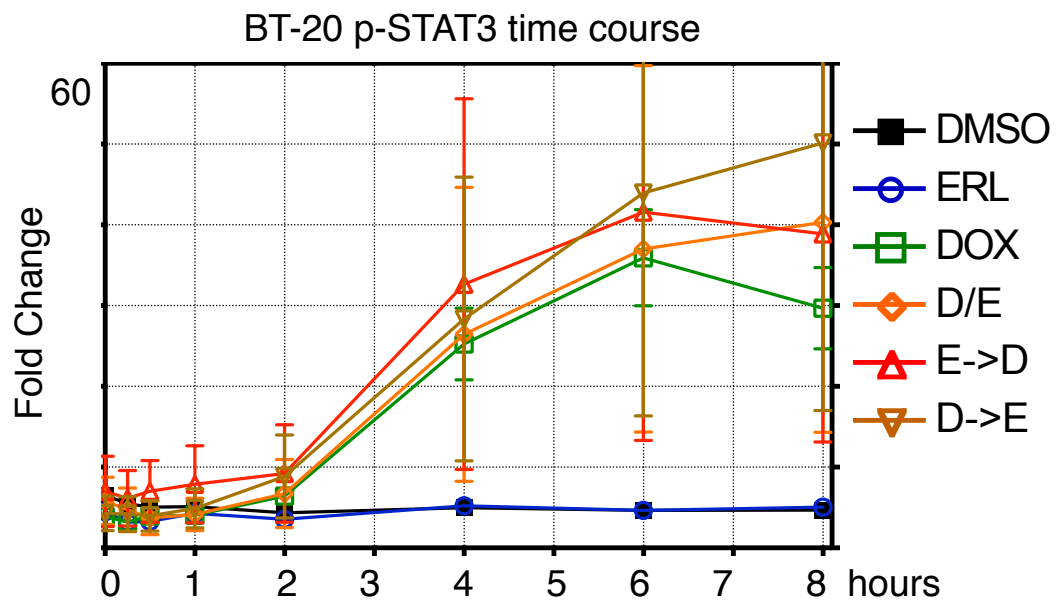


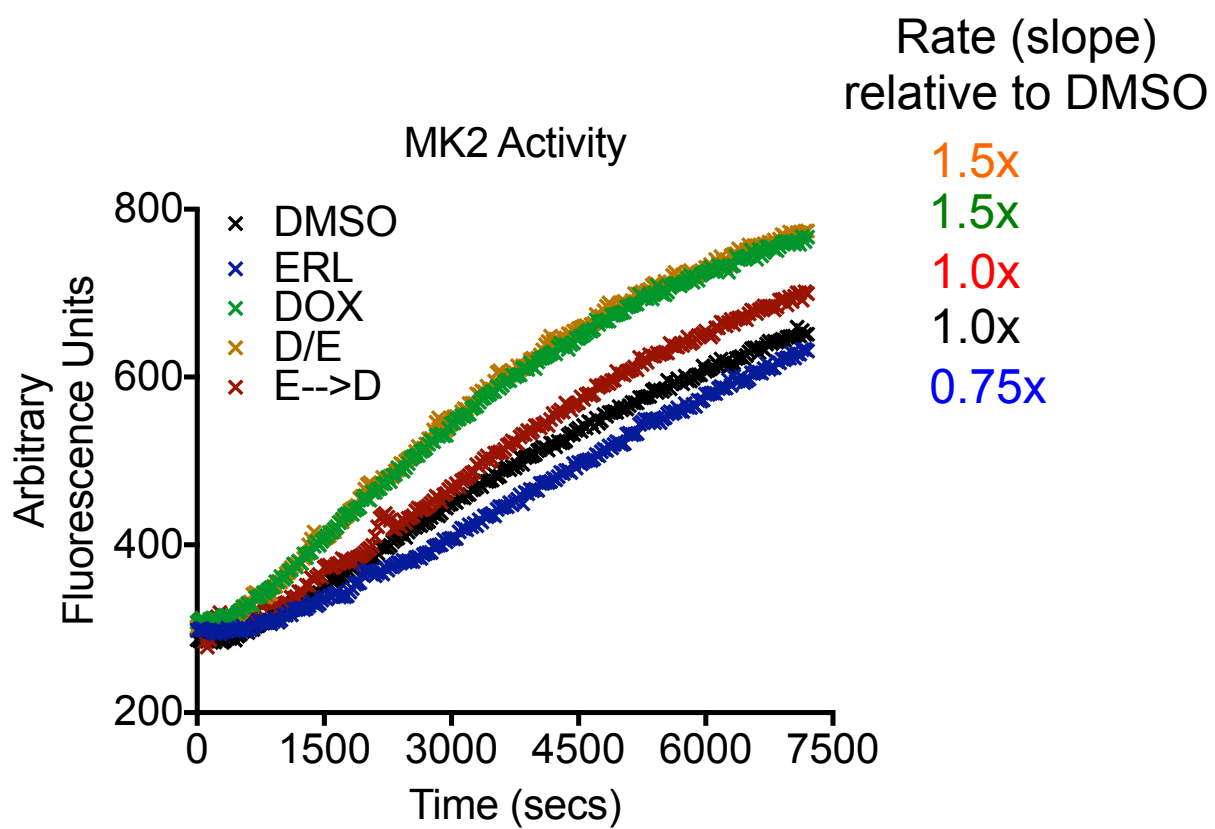


A



B





SUPPORTING DATA

Lee, MJ Table 1

Pathway	Target	Data Format	Pathway	Target	Data Format
ErbB	pMEK	RPMA	Cell Cycle	Cyclin D1	HT-WB
ErbB	pERK	RPMA, KA, HT-WB	Cell Cycle	Cyclin E	RPMA
ErbB	pAKT	RPMA, KA, HT-WB	Cell Cycle	pCDC25C	HT-WB
ErbB	DUSP6	HT-WB	Cell Cycle	p27	HT-WB
ErbB	pJNK	HT-WB	APOP	cIAP1	HT-WB
ErbB	B-RAF	RPMA	APOP	cIAP2	HT-WB
ErbB	p90RSK	RPMA	APOP	XIAP	HT-WB
ErbB	pSEK	RPMA	APOP	BID	HT-WB
ErbB	pABL	HT-WB	APOP	BIM	HT-WB
ErbB	HER2	HT-WB	APOP	SMAC	HT-WB
ErbB	EGFR	HT-WB	APOP	RIP	HT-WB
ErbB	pEGFR	HT-WB	APOP	PUMA	HT-WB
ErbB	PKA	KA	APOP	cC3	FLOW
DDR	pH2AX	RPMA	APOP	cC6	HT-WB
DDR	p53	RPMA	APOP	cC8	HT-WB
DDR	pp53(S15)	HT-WB	APOP	cC9	FLOW
DDR	pp53(S20)	HT-WB	ATG	LC3B	MICROSCOPY
DDR	pCHK1	HT-WB	ATG	Beclin	HT-WB
DDR	pCHK2	HT-WB	ATG	ATG5	WB
DDR	pp38	RPMA	ATG	ATG12	WB
DDR	pDNA-PKcs	RPMA	ATG	4EBP1	RPMA
DDR	pBRCA1	RPMA	ATG	S6K	RPMA
DDR	p53BP1	MICROSCOPY	ATG	S6	RPMA
DDR	MK2	KA	ATG	pSTAT3	HT-WB
DDR	pHSP27	RPMA	ATG	IKBa	HT-WB
Cell Cycle	pHistone H3	RPMA	ATG	pDAPK1	HT-WB
Cell Cycle	pWee1	RPMA	ATG	pDAPK2	HT-WB

FIGURE LEGENDS

Figure 1: Certain Temporal Combinations of Erlotinib and Doxorubicin are Synergistic in Killing TNBC Cells. (A) Schematic of combinations tested. 7 genotoxic drugs and 8 targeted signaling inhibitors were tested in pair-wise combinations, varying dose, order of presentation, dose duration, and dosing schedule. **(B)** Apoptosis in BT-20 cells. Cleaved-caspase 3/cleaved-PARP double positive cells were quantified using flow cytometry. In cells treated with DMSO, erlotinib (ERL) or doxorubicin (DOX), apoptosis measurements were performed 8 hours after drug exposure or at the indicated times. D/E, ERL→DOX, and DOX→ERL refer to DOX and ERL added at the same time, ERL given at the indicated times before DOX, and DOX given at the indicated times before ERL, respectively. For each, apoptotic measurements were made 8 hours after the addition of DOX. Erlotinib and doxorubicin were used at 10 μ M. Mean values \pm S.D. of 3 independent experiments, each performed in duplicate, are shown.

Figure 2: Differentially Expressed Genes Following Erlotinib Treatment in BT-20, MDA-MB-453, and MCF7 Cells. Differentially expressed genes (DEGs) following erlotinib treatment for various amounts of time as indicated. Cells were treated with 10 μ M erlotinib and RNA extracted for microarray analysis. The cut-off for differential gene expression was greater than a 2-fold change and a p-value less than 0.05 (genes that meet both criteria are colored red). P-values were calculated using LIMMA (Smyth, 2004). B score (a measure of significance) is the log of the odds (lods) of differential

expression. Data are from 3 biological replicates. **(A-C)** Time course of erlotinib treatment in BT-20 cells. **(D)** 24 hour erlotinib treatment in MDA-MB-453 cells. **(E)** 24 hour erlotinib treatment in MCF7 cells. Expression data can be found in the GEO repository under the accession number GSE30516.

Figure 3: Long-Term Erlotinib Exposure Re-wires TNBC Cells. DEGs classified using GeneGO “pathway maps”. Heatmap (left) colored according to $-\log(p\text{-value})$; (right) p-value cut-off was 0.05 (dotted red line).

Figure 4: BT-20 Cells are Oncogenically Driven by EGFR Signaling. Microarray analysis using GSEA reveals loss of oncogene signatures in BT-20 cells after sustained EGFR inhibition. RAS Oncogenic Signature and false discovery rate (FDR) adjusted p-values shown **A**. 11 oncogenic signatures from msigdb shown in **B**. Boxes are colored according to normalized enrichment score (NES).

Figure 5: CGN Analysis Identifies ATM and Caspase-8 Networks. Cancer Gene Network Analysis reveals cancer genes likely to be involved in erlotinib-dependent rewiring. Each enrichment chart depicts the normalized enrichment plot (top); the rank of each gene in the network (middle); and the rank ordered gene list (bottom). ATM network shown in (A); Caspase-8 network shown in (B).

Figure 6: Diagram of the EGFR Signaling Pathway. A simplified signaling diagram depicting the canonical EGFR signaling network. Positive (i.e. activating) interactions shown in green; negative (i.e. inhibitory) interactions shown in red.

Figure 7: Analysis of ErbB Signaling Identifies a Subset of Proteins Involved in Time-Dependent ERL/DOX Synergy. The complete ErbB Network signaling dataset for 3 different breast cancer sub-types following combined EGFR inhibition and genotoxic chemotherapy treatments as in Figure 1. Each box represents an 8- or 12-point time course of biological triplicate experiments. Time course plots are colored by response profile, with early/sustained increases in signal colored green, late sustained increases colored red, and transient increases colored yellow. Signals that are not significantly changed by treatment are shaded grey to black with darkness reflecting signal strength. Numbers to the right of each plot report fold-change across all conditions/cells. Data are not shown for signals that did not change in a treatment-dependent or cell line dependent manner. **(B)** Sample detailed signaling time course from panel A, highlighted by dashed box, showing p-ERK activation in BT-20 cells. Mean values \pm S.D. of 3 experiments shown.

Figure 8: Timing of Drug Delivery Does Not Alter DNA Damage Signaling. The complete DDR signaling dataset, colored as in Figure 7. Data are not shown for signals that did not change in a treatment-dependent or cell line dependent manner. **(B)** Sample detailed signaling time course from panel A, highlighted by dashed box,

showing total p53 expression in MCF7 cells. Mean values \pm S.D. of 3 experiments shown.

Figure 9: Long-Term Treatment with Erlotinib Does Not Change Doxorubicin Influx/Efflux or the Level of DNA Damage. Doxorubicin retention measured by flow cytometry. **(A)** Sample time course of BT-20 cells treated with 10 μ M DOX for the indicated times. **(B-D)** Cells treated with doxorubicin (DOX) or pre-treated with erlotinib for 24 hrs. prior to DOX (E \rightarrow D). Cells were collected at 1, 4, or 8 hours after DOX exposure as indicated, and internal doxorubicin fluorescence was measured. **(E-H)** Quantitative microscopy of the early DNA double stranded break response. **(E)** Example image of cells treated with DOX for 1 hour and stained for γ H2AX, 53BP1, or nuclear content (DAPI). **(F-G)** Integrated intensity per nucleus of γ H2AX and 53BP1 foci was measured in BT-20 cells after the indicated treatments and times. Mean values \pm S.D. from triplicate experiments shown. **(H)** Western blot analysis of γ H2AX in BT-20 cells. b-actin shown as a loading control.

Figure 10: Long-Term Treatment with Erlotinib Alters Cell Cycle Progression in MDA-MB-453 But Not Other Cell Lines. Quantitative cell cycle analysis. DNA content and the percentage of mitotic cells were measured by FACS. **(A)** Example FACS plots from untreated BT-20 cells. **(B-D)** Cell cycle stage quantified from 3 experiments, each performed in duplicate. Cells were treated as in Figure 1, and data were collected at 6, 8, 12, 24, and 48 hours after DOX treatment. 8-hour data shown for each cell type. **(E)**

Detailed analysis of cell cycle 24 hours following drug treatment in BT-20 cells. Importantly, timing of drug combination does not significantly alter cell cycle profile in BT-20 cells. Cells were treated as in Figure 1, and cell cycle progress monitored using flow cytometry. Data are mean values \pm S.D. of 3 independent experiments.

Figure 11: Modulation of Cell Cycle Does Not Play a Prominent Role in ERL→DOX Sensitivity. The complete Cell Cycle signaling dataset, colored as in Figure 7. Data are not shown for signals that did not change in a treatment-dependent or cell line dependent manner. **(B)** Sample detailed signaling time course from panel A, highlighted by dashed box, showing p-Wee1 levels in MDA-MB-453 cells. Mean values \pm S.D. of 3 experiments shown.

Figure 12: Apoptotic Signaling is Robustly Changed in Time-Dependent Combination Treatments. The complete Apoptotic Network signaling dataset, colored as in Figure 7. Data are not shown for signals that did not change in a treatment-dependent or cell line dependent manner. **(B)** Sample detailed signaling time course from panel A, highlighted by dashed box, showing cleaved-caspase-8 levels in BT-20 cells. Mean values \pm S.D. of 3 experiments shown.

Figure 13: Enhanced Sensitivity to Doxorubicin is Mediated by Caspase-8 Activation. Apoptosis measured 8 hours after the indicated treatment in cells expressing control RNA (scrambled siRNA) or caspase-8 specific siRNA in BT-20. Cells

were exposed to 5 nM siRNA for 48-hours, then treated as in Figure 1. **(A)** Western blot verifying caspase-8 knockdown in BT-20. **(B)** Percent Apoptotic Cells, as measured in Figure 1. Apoptotic values represent mean response \pm S.D. from both siRNAs, each in duplicate.

Figure 14: Doxorubicin Induces an Increase in Pro-Autophagic Signaling and Autophagic Flux. The complete Autophagic/Metabolic Network signaling dataset, colored as in Figure 7. Data are not shown for signals that did not change in a treatment-dependent or cell line dependent manner. **(B)** Sample detailed signaling time course from panel A, highlighted by dashed box, showing p-STAT3 levels in BT-20 cells. Mean values \pm S.D. of 3 experiments shown.

Figure 15: *In vitro* Kinase Assays Reveal a Role for Loss of MK2 Signaling in Enhanced Sensitivity to Doxorubicin. MK2 activity measured using a fluorescent MK2 substrate probe. Probes were designed using peptide sequences that match the optimal substrate motif for MK2. Upon phosphorylation of the peptide probe, fluorescence is increased. Cell lysates were created at various times after drug treatment, and activities of ERK, AKT, MEK, MEF2, PKA, and MK2 were measured. Data for MK2 shown. Data are from 2-hour treatment lysates. DOX or D/E induce MK2 activity. ERL reduces MK2 activity. MK2 activity in the E \rightarrow D condition is similar to vehicle control (DMSO).

Table 1: Protein Targets of Interest and Source of Data Production. Table 1 shows the protein targets that were monitored in this study, and the source of data production. Targets that were deemed of interest for future analyses are colored red. RPMA = reverse phase protein microarray. HT-WB = high-throughput western blot. WB = western blot. KA = kinase assay.